2-D hp adaptive control volume isogeometric analysis based on hierarchical Fup basis functions

G. Kamber[a], H. Gotovac[a], V. Kozulić[a], B. Gotovac[a]

[a]*Faculty of Civil Engineering, Architecture and Geodesy, University of Split, Matice hrvatske 15, 21000 Split, Croatia*

Abstract

In this paper, 2-D hp adaptive procedure is developed based on Control Volume Isogeometric Analysis (CV-IGA) and Hierarchical Fup (HF) basis functions. Contrary to the most common truncated hierarchical splines, HF enables hp adaptation because higher resolution levels do not include only basis with smaller compact support or higher frequencies, but also with higher order. Consequence of this property is spectral convergence of the proposed adaptive algorithm which is presented on classical benchmarks such as L-shape benchmark and advection dominated problems. Even in non-smooth problems, spectral convergence is achieved contrary to the application of uniform grid. CV-IGA ensures local and global mass conservation which is potentially very important for fluid mechanics problems. 2-D proposed algorithm chooses regular control volumes in parametric space at all resolution levels closely related to the Greville points (vertices) of basis functions. Therefore, methodology is very simple requiring only overlapping of control volumes in the areas where different levels are connected, while its computational cost lies between Galerkin and collocation formulations.

Keywords: Hierarchical Fup Basis Functions, hp-refinement, Local Refinement, Control Volume, Isogeometric Analysis, Adaptive Methods

Contents

1. Introduction

Many industrial and real applicative problems in computational mechanics have been solved by numerical simulations that require large computational resources including parallel computing and the use of CPU/GPU clusters and/or supercomputers. Therefore, it is of great importance that computer resources are used as efficiently as possible.

Numerical modeling of different physical and engineering problems characterized with large range of spatial and temporal scales are typically faced by many difficulties. Many different numerical approaches and methods have been proposed in recent decades. In general, each method has its advantages, but also disadvantages, and none can be singled out as the best for all problems. The classical methods are finite element method (FEM), finite difference method (FDM) and finite volume method (FVM) [1, 2, 3, 4, 5, 6, 7, 8, 9]. There are various other methods such as the spectral element method (SEM), boundary element method (BEM) [10], discrete element method (DEM) [11] which, together with various collocation, meshfree and other hybrid approaches, are usually practical for limited classes of problems.

The gap between computer-aided design (CAD) for the geometry description on the one hand and finite element analysis (FEA) for the solution description on the other hand has been long evident, and mostly present due to differences in the used interpolation (basis) functions. Whereas classical polynomials have dominated in the field of numerical analysis, spline-based basis functions (e.g., B-splines, non-uniform rational B-splines (NURBS) [12],

T-splines [13], hierarchical B-splines (HB) [14] etc.) play a crucial role in the field of computational geometry. True popularity of spline functions for numerical analysis was achieved by the introduction of the concept of isogeometric analysis (Hughes *et al.* [12] and Cottrell *et al.* [15]). The main idea of isogeometric analysis (IGA) is to bridge the gap between FEA and a CAD by using the same type of spline basis functions for both systems. Therefore, IGA allows accurate representation of geometry in CAD terms in contrast to classical FEA where geometry is only approximated.

IGA is closely related to the meshless or mesh-free methodologies due to its use of spline basis functions. Application of spline basis functions enables some properties not seen in FEM, such as exact geometry description, no cumbersome meshing, usage of higher-order basis functions, higher continuity of solution and geometry, more efficient refinement adaptive procedures and multiresolution approach [16]. Efficient numerical modeling using spline functions does not always have to be associated exclusively with IGA involving geometry transformations, because everything can only be performed in the physical domain which is immersed to the background mesh defined on regular rectangle in 2-D or cube in 3-D (see for instance immersogeometric methods in Hsu *et al.* [17], Rvachev structure method by Rvachev *et al.* [18] or WEB-splines by Höllig *et al.* [19]).

The development of adaptive methods [20, 21, 22, 23] for local refinement and coarsening became one of the most important researched topics within IGA. Since a fundamental limitation of traditional NURBS is the lack of potential for local refinement, several solutions have been derived, such as T-splines [13, 24, 25, 26, 27, 28, 29], hierarchical B-splines (HB) [14], truncated hierarchical B-splines (THB) [30, 31, 32, 33, 34] and locally refined B-splines (LR) [35]. Furthermore, linear independence, stability and partition of unity as well as local refinement and adaptation became center topics for these adaptive solutions.

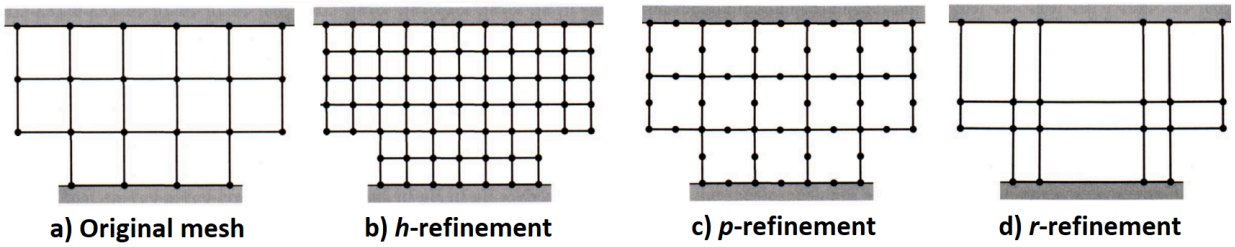

Figure 1: Refinement procedures.

Adaptive isogeometric methods attract a lot of attention and are a very active field of research which can generally be divided to h-refinement (Figure 1b; spline functions of the

same order but smaller knot intervals, i.e. higher frequencies), p-refinement (Figure 1c; higher degree of basis functions), r-refinement (Figure 1d; redesigning the mesh without changing the number of nodes and only adjusting their positions) and their combinations. Even though B-splines and NURBS are most commonly used spline technologies in the isogeometric settings, due to their tensor product structure, they are not well suited to treat localized phenomena. Hierarchical B-splines (HB) constitute one of the most promising solutions to easily define adaptive spline grid which preserve the non-negativity of standard B-splines and enables the possibility to properly deal with local problems [14]. However, since the hierarchical B-spline basis functions in non-rational form do not satisfy partition of unity, it may produce ill-conditioned control meshes at the refined level [30]. To overcome this deficiency, the truncated mechanism was first developed by Giannelli *et al.* [14] for the hierarchical B-spline basis functions (THB) to form a partition of unity and to decrease the overlapping of basis functions for better numerical conditioning.

In addition to spline functions, relatively lesser-known atomic basis functions have been used in recent times (see Rvachev and Rvachev [36] and Gotovac [37]). Atomic basis functions can be placed between classical polynomials and spline functions. However, in practice, their use as basis functions is closer to splines or wavelets (see Beylkin and Keiser [38]). Gotovac [37] systematizes the existing knowledge about atomic basis functions and transforms them into a numerically appropriate form, especially Fup basis functions as a typical member of atomic class of basis functions. Kozulić [39] and Gotovac and Kozulić [40] showed the basic possibilities of using Fup basis functions in structural mechanics and numerical analysis. The use of Fup basis functions has been shown to solve the problem of signal processing (see Kravchenko *et al.* [41]), the initial problem (see Gotovac and Kozulić [42]) and the boundary problems using the non-adaptive Fup collocation method (see Kozulić and Gotovac [43] and Gotovac *et al.* [44]).

Gotovac *et al.* [45] presented a true multiresolution approach based on the Adaptive Fup Collocation Method (AFCM). The heart of the AFCM methodology lies in the Fup basis functions in conjunction with the collocation procedure. However, the main drawback was the lack of global and local mass balance due to the properties of the collocation framework and inability to describe the general irregular geometry. Malenica *et al.* [46] firstly developed Control Volume Isogometric Analysis (CV-IGA) applied to the karst groundwater flow model, while Gotovac *et al.* [16] presented CV-IGA in the context of other Galerkin and collocation formulations. Kamber *et al.* [47] set foundation for efficient adaptive spatial procedure developing 1-D hierarchical Fup (HF) basis functions inside CV-IGA. HF have

the option of local hp-refinement such that they can replace certain Fup basis functions at one resolution level with new basis functions at the next resolution level that have a smaller length of the compact support (h-refinement) but also higher order (p-refinement).

In this work, we present a novel adaptive algorithm that is based on hierarchical 2-D Fup basis functions and CV-IGA, which are closely related to the HB and THB. HF provides spectral convergence and presents a substantial improvement in comparison to THB that enable only polynomial convergence.

2. Spline basis functions

2.1. Hierarchical B-spline basis functions

The B-spline basis functions are piecewise polynomial functions defined in parametric space. B-spline basis functions are defined recursively (see Cottrell *et al.* [15]) starting with piecewise constants ($n = 0$):

$$B_{i,0}(\xi) = \begin{cases} 1 & \xi_i \leq \xi < \xi_{i+1} \\ 0 & elsewhere \end{cases} \tag{1}$$

and for $n > 0$, B-splines are defined by

$$B_{i,n}(\xi) = \frac{\xi - \xi_i}{\xi_{i+n} - \xi_i} B_{i,n-1}(\xi) + \frac{\xi_{i+n+1} - \xi}{\xi_{i+n+1} - \xi_{i+1}} B_{i+1,n-1}(\xi). \tag{2}$$

Figure 2 presents B-spline basis functions for $n = 0, 1, 2$ on a uniform knot vector. An interesting fact is that standard piecewise constant and linear finite element functions are the same for $n = 0, 1$. However, for higher-orders of B-spline basis functions they differ from their FEA counterparts.

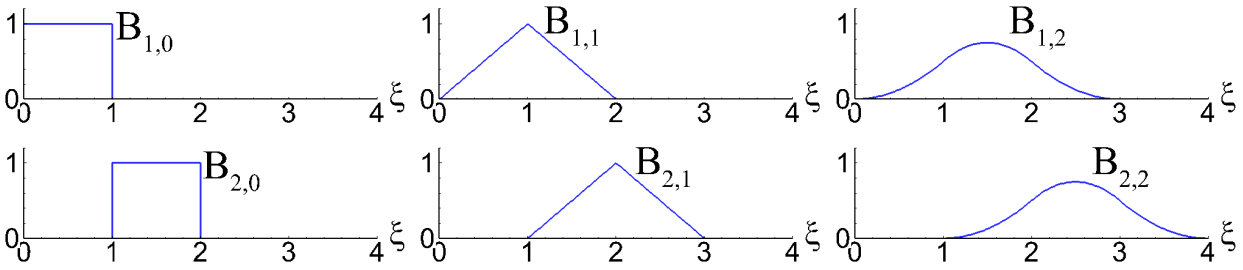

Figure 2: Basis functions of order $0, 1$, and 2 for uniform knot vector $\Xi = \{0, 1, 2, ...\}$.

$B_n(\xi)$ can be presented by using convolution theorem in the following form:

$$B_n(\xi) = \int_{-\infty}^{\infty} B_{n-1}(\xi - t)\, B_0(t)\ dt \tag{3}$$

or:

$$B_n(\xi) = B_{n-1}(\xi) * B_0(\xi) = \underbrace{B_0(\xi) * ... * B_0(\xi)}_{(n+1)\quad times} \tag{4}$$

where n is the order of the B-spline. The convolution theorem states that the Fourier transform (FT) of $B_n(\xi)$ can be expressed as a product of $(n+1)$ particular FT's of $B_0(\xi)$ according to (4):

$$f_n(t) = \left(\frac{sint/2}{t/2}\right)^{n+1} \tag{5}$$

so the inverse FT of $B_n(\xi)$ is defined by:

$$B_n(\xi) = \frac{1}{2\pi} \int_{-\infty}^{\infty} \left(\frac{sin\,(t/2)}{t/2}\right)^{n+1} \cdot e^{-it\xi} dt. \tag{6}$$

Equation (4) implies that the support of $B_n(\xi)$ is the union of the $(n+1)$ characteristic intervals $\Delta\xi$. By increasing the B-spline order, the length of its compact support also increases, and when $n \to \infty$, the length goes to infinity. The coordinate ξ_T is called the vertex of the basis function (point with maximum function value) and serves as the origin for the shifting of the basis functions along the ξ axis by the length of the characteristic interval.

In one-dimensional problems, a knot vector is a set of non-decreasing real numbers representing coordinates in the parametric space of the curve

$$\Xi = \{\xi_1, \xi_2, ..., \xi_{n+p+1}\} \tag{7}$$

where ξ_i is the i-th knot, i is the knot index, $i = 1, 2, ..., n+p+1$, n is the polynomial order of the B-spline, and p is the number of basis functions which comprise the B-spline. The interval $[\xi_1, \xi_{n+p+1}]$ is called a patch. If knots are equally-spaced in the parametric space, they are said to be uniform, otherwise they are non-uniform. More than one knot can be located at the same coordinate in the parametric space, and are referred to as repeated knots. A knot vector is said to be open if its first and last knots appear $p+1$ times. $B_n(\xi)$ is presented by the local polynomial of the n-th order on each interval $[\xi_k, \xi_{k+1}]$.

We can summarize the properties of the B-splines basis functions as follows:

1. B_n-spline is positive on $n+1$ characteristic intervals and vanishes outside this interval i.e., B-splines have compact support where they have strictly positive non-zero values; elsewhere, they are zero, implying localized approximation properties.
2. B_n-spline is $(n-1)$-times continuously differentiable with discontinuities of the n-th derivative.
3. A linear combination of shifted B_n-splines by a characteristic interval describes algebraic polynomials up to the n-th order.
4. A linear combination of m shifted B-splines by a characteristic interval describes a unit constant function ("partition of unity"), that is

$$\sum_{i=1}^{m} B_{i,n}(\xi) = 1 \tag{8}$$

5. B_n-splines can be presented by a linear combination of the shifted B-splines of the same order, but using two-times-smaller support. This implies that B-splines support multiresolution analysis and efficient adaptive numerical procedures (e.g., [20, 21, 22, 23, 24, 30, 31, 33, 32]).

B-spline basis functions are refinable, which enables the construction of HB and its truncated variant THB. Truncated hierarchical B-splines (THB) were introduced and analysed in [14, 48]. THB-splines can be considered as an upgrade for hierarchical B-splines (HB) i.e., an alternative base for the space of hierarchical splines, that retains the partition of unity property and reduces the support of the basis functions, therefore reducing the interaction between them. In the classical hierarchical construction, coarse basis functions of a certain level l whose support is completely covered by finer basis functions of level $l+1$ are replaced. However for THB, the replacement is done as in the hierarchical case with addition that coarse basis functions whose support has a non-empty overlap with the domain Ω^{l+1} are truncated (see Figure 3).

THB refinability (see [14, 30]) indicates that a basis function B_n^l defined on Ξ^l can be represented as a linear combination of $n+2$ B_n^{l+1} basis functions defined on Ξ^{l+1} as,

$$B_{i,n}^l(\xi) = \sum_{k=0}^{n+1} c_{i,k}^n B_{2i+k,n}^{l+1}(\xi) \quad \text{with} \quad c_{i,k}^n = \frac{1}{2^n}\binom{n+1}{k}, i = 0, ..., m^l - 1 \tag{9}$$

where $c_{i,k}^n$ are the refinement coefficients and m^l is the number of basis functions defined on Ξ^l. This procedure enables h-adaptive methods because each next resolution level has basis functions with two times smaller compact support (h-refinement).

The $n+2$ basis functions $B^{l+1}_{2i+k,n}$ on the next level are called the children of $B^l_{i,n}(\xi)$ i.e., denoted as,

$$chdB^l_{i,n}(\xi) = \left\{ B^{l+1}_{2i+k,n}(\xi) | k = 0, 1, ..., n+1 \right\}. \tag{10}$$

In the following, construction of only two consecutive levels with basis functions from level l and $l+1$ will be shown, where $l \geq 0$. Starting from the initial parametric domain Ω^l with equally spaced knots $\Xi^l = \{0, 1, 2, 3, 4, 5, 6, 7, 8, 9, 10\}$, $\mathcal{B}^l$ set of B-spline basis functions are defined on a level l (see Figure 3). The supports of all the basis functions $\mathcal{B}^l$ from initial level l covers Ω^l i.e., $\Omega^l = supp\ B^l$. According to [49], the function space spanned by $\mathcal{B}^l$ can be enlarged by replacing the certain B-spline basis functions with their children, which indicates a local refinement of basis functions. Figure 3 shows a construction process for univariate cubic THB in three steps:

- Identify a set of basis functions $\mathcal{B}^l_p \subseteq \mathcal{B}^l$ to be refined at level l (gray solid curve) and designate them as *passive* while the remaining basis functions in $\mathcal{B}^l$ are designated as *active* ($\mathcal{B}^l_a = \mathcal{B}^l \setminus \mathcal{B}^l_p$).

- Obtain the children at level $l+1$ (red solid curves) only for the *passive* $\mathcal{B}^l_p$ and define them as *active*; $\mathcal{B}^{l+1}_a = chd\mathcal{B}^l_p$.

- Merge all of the basis functions that are *active* from levels l and $l+1$ to obtain the hierarchical B-spline basis functions on the new level,

$$\mathcal{B}^{l+1}_{hbf} = \mathcal{B}^{l+1} = \mathcal{B}^l_a \cup \mathcal{B}^{l+1}_a. \tag{11}$$

Eq. (11) refers to the global selection of all active basis functions, where the active basis functions are updated in each recursive step described above. Hierarchical B-spline basis functions in nonrational form do not satisfy partition of unity. To overcome that problem and to decrease the overlapping of basis functions for better numerical conditioning, a truncated mechanism for hierarchical B-splines was developed [14, 30]. Figure 3 shows how in the classical hierarchical construction, coarse basis functions from level l whose support is completely covered by finer B-splines of level $l+1$ are replaced. THB-splines refinement (replacement) works as in the hierarchical case with addition of active coarse basis functions $\mathcal{B}^l_a$ whose supports have a non-empty overlaps with Ω^{l+1}. These functions need to be modified or truncated as follows.

Definition. *Given a set of (passive) basis functions $\mathcal{B}^l_p$ to be refined, refinement area is defined as $\Omega^{l+1} = supp\mathcal{B}^l_p$. Provided that $B^l_i \notin B^l_p$ is refinable and following Eq.* (9) *for its*

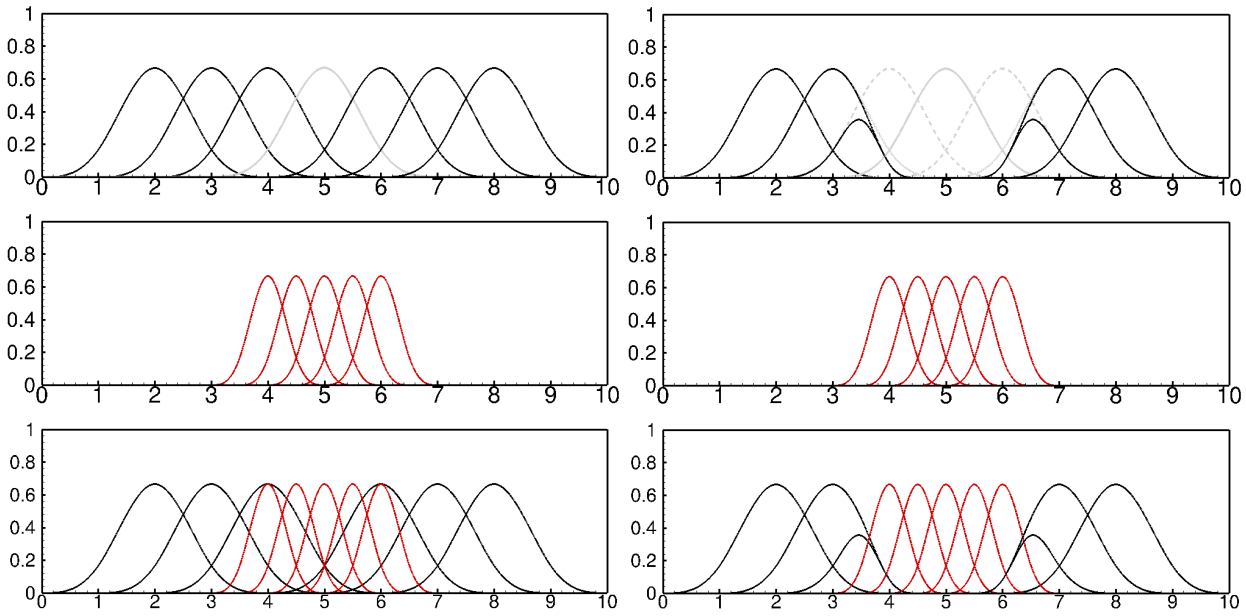

(a) HB-splines on level l and $l+1$

(b) THB-splines on level l and $l+1$

Figure 3: Comparison of univariate cubic HB- and THB-splines. (a) Three steps to construct univariate cubic HB-spline basis function without truncation and (b) tree steps to construct univariate cubic HB-spline basis function with truncation (THB).

refinability gives,

$$B_i^l(\xi) = \sum_{suppB_j^{l+1} \subseteq suppB_i^l} c_{i,j} B_j^{l+1}(\xi), \tag{12}$$

where $c_{i,j} \in \mathbb{R}$ *are refinement coefficients from mid-knot insertions, and* $\mathcal{B}_j^{l+1}(\xi) \in chdB_i^l(\xi)$. *The truncated basis function* $\mathcal{B}_i^l$ *is defined as*

$$trunB_i^l(\xi) = \sum_{suppB_j^{l+1} \nsubseteq \Omega^{l+1}} c_{i,j} B_j^{l+1}(\xi) \tag{13}$$

with respect to $\mathcal{B}_p^l$ [30].

Equation (13) indicates that only children of $\mathcal{B}_i^l$ whose supports are fully contained in Ω_{l+1} are discarded while constructing the truncated basis function $trunB_i^l$. In Figure 3, the gray solid line represents the basis function to be refined $\mathcal{B}_p^l$ which is also set as passive, and refinement area is $\Omega^{l+1} = [3, 7]$. In case for univariate cubic hierarchical B-splines, each basis function from level l has five children on level $l+1$, and four basis functions surrounding $\mathcal{B}_p^l$ (2 on the left and 2 on the right side; gray dashed curve) need to be truncated because they have children with supports fully contained in Ω^{l+1}. For the two basis functions adjacent to

$\mathcal{B}_p^l$ three children are discarded, and for the other two basis functions, only one children is discarded. Basis functions that are far away from refinement area Ω^{l+1} i.e., they do not have children within that area, are not truncated. After truncating all designated basis functions, new level is constructed by combining active functions from level l (black solid curve and gray dashed curve; non-truncated and truncated) with active basis functions from level $l+1$ (red solid curve; $\mathcal{B}_a^{l+1} = chd\mathcal{B}_p^l$).

The hierarchical B-spline basis with truncation has been proven to form a partition of unity and therefore achieves strong stability [48]. It gives a sparser connectivity among basis functions at different levels, and it can preserve geometry when local refinement is performed [30].

2.2. Hierarchical Fup basis functions

Fup basis functions belong to the class of atomic functions (see [36],[40]) and span vector space of algebraic polynomials, while their properties are closely related to the B-splines, as will be explained in the sequel.

Function $up\,(\xi)$ can be obtained by an infinite number of convolutions of the contracted $B_0\,(\xi)$ with compact support 2^{-k} and vertex value 2^k, $k \in \mathbb{N}$, according to following convolution procedure:

$$up\,(\xi) = B_0\,(\xi) * B_0\,(2\xi) * \cdots * B_0\left(2^k\xi\right) * \cdots * B_0\,(2^\infty\xi) \tag{14}$$

From (14), the compact support of $up\,(\xi)$ is the union of an infinite number of finite intervals. However, its compact support is finite:

$$h_{up} = \sum_{k=0}^{\infty} \frac{1}{2^k} = 2 \qquad \rightarrow \qquad \text{supp } up\,(\xi) = [-1,\ 1] \tag{15}$$

The convolution procedure (14) causes $up(\xi)$ to contain all polynomial orders by parts of its compact support. Due to its infinite number of continuous and non-zero derivatives, function $up(\xi)$ can be regarded as a perfect spline.

The values of $up(\xi)$ and its derivatives can be found exactly in the form of rational numbers in the binary-rational points. Those binary-rational points are defined as:

$$\xi_{br} = -1 + k \cdot 2^{-m}, \quad m \in N, \quad k = 1,\ \ldots, 2^{m+1}. \tag{16}$$

At all other points of the compact support calculation of $up\,(\xi)$ can be done only approximately, but up to the computer accuracy.

For the calculation of $up(\xi)$ values at arbitrary points, Gotovac and Kozulić [40] suggested a special series based on Taylor series of the $up(\xi)$ function at the binary-rational points ξ_{br} (because it is then a polynomial of the n-th order). Values of the even function $up(\xi)$ in arbitrary point $\xi \in [0,1]$ can be presented as follows:

$$up\,(\xi) = 1 - up(\xi - 1) = 1 - \sum_{k=1}^{\infty} \; (-1)^{1+p_1+\cdots+p_k} \; p_k \sum_{j=0}^{k} C_{jk} \cdot {\Delta_k}^j \tag{17}$$

where the coefficients C_{jk} are rational numbers containing values of $up(\xi)$ at the binary-rational points $\xi_k = -1 + 1/2^m$ [40]:

$$C_{jk} = \frac{1}{j!} 2^{j(j+1)/2} up(-1 + 2^{-(k-j)}) \; ; \quad j = 0 \; , \; 1 \; , \; \ldots \; , \; k \; \; ; \; \; k = 1 \; , \; 2 \; , \; \ldots \; , \; \infty \tag{18}$$

Factor Δ_k in (17) presents the difference between the real value of coordinate ξ and its binary presentation with k bytes, where $p_1 \ldots \; p_k$ are the digits 0 or 1:

$$\Delta_k = \xi - \sum_{i=1}^{k} p_i \cdot \frac{1}{2^i} \tag{19}$$

For an exact description of polynomials up to the n-th order on the interval $\Delta\xi_n = 2^{-n}$, it is necessary to use 2^{n+1} basis functions obtained by shifting $up(\xi)$ for $\Delta\xi_n$. Such a relatively large number of basis functions implies poor approximation properties of $up\,(\xi)$. This is the main reason why application of $up(\xi)$ in numerical analysis for practical purposes is quite limited.

$Fup_n(\xi)$ are another class of atomic basis functions, also belonging to the polynomial types of basis functions, which require only $(n{+}2)$ basis functions to exactly describe polynomials up to the n-th order on interval $\Delta\xi_n = 2^{-n}$. For instance, for the development of a 4-th order polynomial, only 6 or $(n{+}2)$ functions $Fup_4(\xi)$ are needed in comparison to 32 $up(\xi)$ basis functions. The compact support of $Fup_n(\xi)$ contains $n{+}2$ characteristic intervals $\Delta\xi_n = 2^{-n}$:

$$supp \;\; Fup_n(\xi) = \left[-\,(n{+}2) \cdot 2^{-n-1}, \;\; (n{+}2) \cdot 2^{-n-1} \right] \tag{20}$$

For $n = 0$, the following holds:

$$Fup_0(\xi) = up(\xi) \tag{21}$$

Function $Fup_n(\xi)$ can be obtained by a convolution procedure using the contracted B_n and up basis function:

$$Fup_n(\xi) = B_n(2^n \; \xi) * up \; (2^{n+1} \; \xi) \tag{22}$$

This means that $Fup_n(\xi)$ is closely related to $B_n(\xi)$ and that they together share all the mentioned properties. However, $Fup_n(\xi)$ has better approximation properties than $B_n(\xi)$ due to the convolution with the *up* function containing all orders of polynomials by parts and infinite continuity. Moreover, they share the same convergence properties because it is directly linked by the polynomial order which can be exactly described by linear combination of these functions. Additionally, the $Fup_n(\xi)$ has better approximation properties which are paid by one more characteristic interval for the same n-th order of basis functions. Equation (22) is not numerically favorable for calculating the value of the function $Fup_n(\xi)$.

Atomic basis functions have a "deeper" mathematical background, and they are generally solutions of differential-functional equations, which for $Fup_n(\xi)$ take the following form:

$$Fup_n^{'}(\xi) = 2\sum_{k=0}^{n+2}\left(C_n^k - C_n^{k-2}\right)\cdot Fup_n\left(2\xi - \frac{k}{2^n} + \frac{n+2}{2^{n+1}}\right) \tag{23}$$

where C_n^k are binomial coefficients defined as

$$C_n^k = \binom{n}{k} = \frac{(n)!}{(n-k)!\cdot k!} \tag{24}$$

Equation (23) presents the atomic structure of these basis functions because its derivatives (but also a function values as will be shown in the sequel) are decomposed by a linear combination of these same functions (Rvachev and Rvachev [36]). $Fup_n(\xi)$ can be calculated by a linear combination of $up(\xi)$ mutually shifted by the characteristic interval 2^{-n}:

$$Fup_n(\xi) = \sum_{k=0}^{\infty} C_k(n)\cdot up\left(\xi - 1 - \frac{k}{2^n} + \frac{n+2}{2^{n+1}}\right) \tag{25}$$

The zero coefficient in (25) is:

$$C_0(\mathrm{n}) = 2^{C_{n+1}^2} = 2^{n(n+1)/2} \tag{26}$$

Other coefficients are calculated in the form $C_k(n) = C_0(n)\cdot C_k^{'}(n)$, where the coefficients $C_k^{'}(n)$ are obtained using the following recursive formulas:

$$\begin{aligned} C_0^{'}(n) &= 1 \\ C_k^{'}(n) &= (-1)^k C_{n+1}^k - \sum_{j=1}^{min\left\{\ k\ ;\ 2^{n+1}-1\right\}} C_{k-j}^{'}(n)\cdot\delta_{j+1} \end{aligned} \tag{27}$$

In the numerical modeling of boundary value problems, there is a need to modify boundary basis functions in order to keep the same approximation properties as inside the domain. The concept of boundary basis functions refers to the linear combination of basis functions whose compact supports are at least partially located inside the domain. For simpler notation, modified boundary Fup_n basis functions are designated as $\varphi_{n,j}$, $j = -[(n+1)/2], ..., [n/2]$ on the left domain boundary ξ_A, and $j = N - [n/2], ..., N + [(n+1)/2]$ on the right domain boundary ξ_B (N is the number of characteristic intervals $\Delta\xi_n$ inside the domain).

The boundary basis functions $\varphi_{n,j}$ on the left domain boundary are modified so that i-th derivation is satisfied in a manner

$$\begin{aligned} &\varphi_{n,j}^{(i)}(\xi_A) \neq 0 \quad for \quad j + [(n+1)/2] \leqslant i \leqslant n \\ &\varphi_{n,j}^{(i)}(\xi_A) = 0 \quad otherwise; \qquad\qquad i \in \mathbb{N} \end{aligned} \tag{28}$$

Modification of the right boundary basis functions is achieved by translating and mirroring the left modified boundary basis functions. In the vector space of mutually displaced Fup_n basis functions, it is necessary to modify the $(n+1)$ basis functions on each boundary.

We can summarize the properties of the Fup basis functions as follows:

1. Fup_n is positive on $n+2$ characteristic intervals and vanishes outside these intervals i.e., Fup basis functions have compact support where they have strictly positive non-zero values; elsewhere, they are zero, implying localized approximation properties.
2. Fup_n is infinitely differentiable.
3. A linear combination of m shifted Fup basis functions by a characteristic interval describes a unit constant function ("partition of unity"), that is

$$\frac{1}{2^n} \sum_{i=1}^{m} Fup_{i,n}(\xi) = 1 \tag{29}$$

4. Fup_n can be presented by a linear combination of the shifted Fup basis functions with the higher order, but using two-times-smaller supports. This implies that Fup basis functions enable multiresolution analysis and efficient adaptive numerical procedures (e.g., [47]).

Basis function Fup_n^l defined on Ξ^l can be represented as a linear combination of $n+2$ Fup_{n+1}^{l+1} basis functions defined on Ξ^{l+1},

$$Fup_n^l(\xi) = \sum_{k=0}^{n+1} C_{n+1}^k \cdot Fup_{n+1}^{l+1}\left(\xi - \frac{k}{2^{n+1}} + \frac{n+1}{2^{n+2}}\right), \tag{30}$$

where C_{n+1}^{k} are the refinement coefficients

$$C_{n+1}^{k} = \frac{1}{2^{n+1}} \binom{n+1}{k} \tag{31}$$

The $n+2$ basis functions Fup_{n+1}^{l+1} are called the *children* of Fup_{n}^{l}, denoted as

$$chdFup_{n}^{l}(\xi) = \left\{ Fup_{n+1}^{l+1}\left(\xi - \frac{k}{2^{n+1}} + \frac{n+1}{2^{n+2}}\right) \middle| k = 0, 1, ..., n+1 \right\} \tag{32}$$

In contrast to THB, hierarchical Fup basis functions (HF) enable *hp*-adaptive methods because each next resolution level not only decreases compact support, but also increases the order of the basis functions (*hp*-refinement).

At the zero coarsest level, we can define a set of uniformly distributed Fup basis functions $\mathcal{F}^0$. The initial domain is covered with the compact supports of all the Fup basis functions in $\mathcal{F}^0$ i.e., $\Omega^0 = supp\mathcal{F}^0$. Since Fup basis functions are refinable, it indicates that the function space spanned by $\mathcal{F}^0$ can be enlarged by replacing the selected Fup basis functions with their children (see Eq. (30)) [40]. In the following, we will show only two consecutive levels and construct level $l+1$ from the level l.

Figure 4 illustrates the construction process of hierarchical Fup basis functions in three steps:

- Identify a set of basis functions $\mathcal{F}_{p}^{l} \subseteq \mathcal{F}^{l}$ to be refined at level l (black dashed curve) and designate them as *passive* while the remaining basis functions in $\mathcal{F}^{l}$ (black solid curves) are designated as *active* ($\mathcal{F}_{a}^{l} = \mathcal{F}^{l} \setminus \mathcal{F}_{p}^{l}$).

- Obtain the children at level $l+1$ (red solid curves) only for the *passive* Fup_{n}^{l} and define them as *active*; $\mathcal{F}_{a}^{l+1} = chd\mathcal{F}_{p}^{l}$.

- Merge all of the basis functions that are *active* from levels l and $l+1$ to obtain the hierarchical Fup basis functions,

$$\mathcal{F}_{hbf}^{l+1} = \mathcal{F}^{l+1} = \mathcal{F}_{a}^{l} \cup \mathcal{F}_{a}^{l+1}. \tag{33}$$

Hierarchical Fup basis functions satisfy partition of unity such that every Fup_n basis function on the zero coarsest level is multiplied with constant 2^{-n} (see Eq. (29)). Since every Fup_{n}^{l} basis function defined on the level l can be represented as a linear combination of $n+2$ Fup_{n+1}^{l+1} basis functions defined on the level $l+1$ (see Eq. (30)), it entails that all of the Fup basis functions that are created at higher resolution levels also satisfy partition of unity.

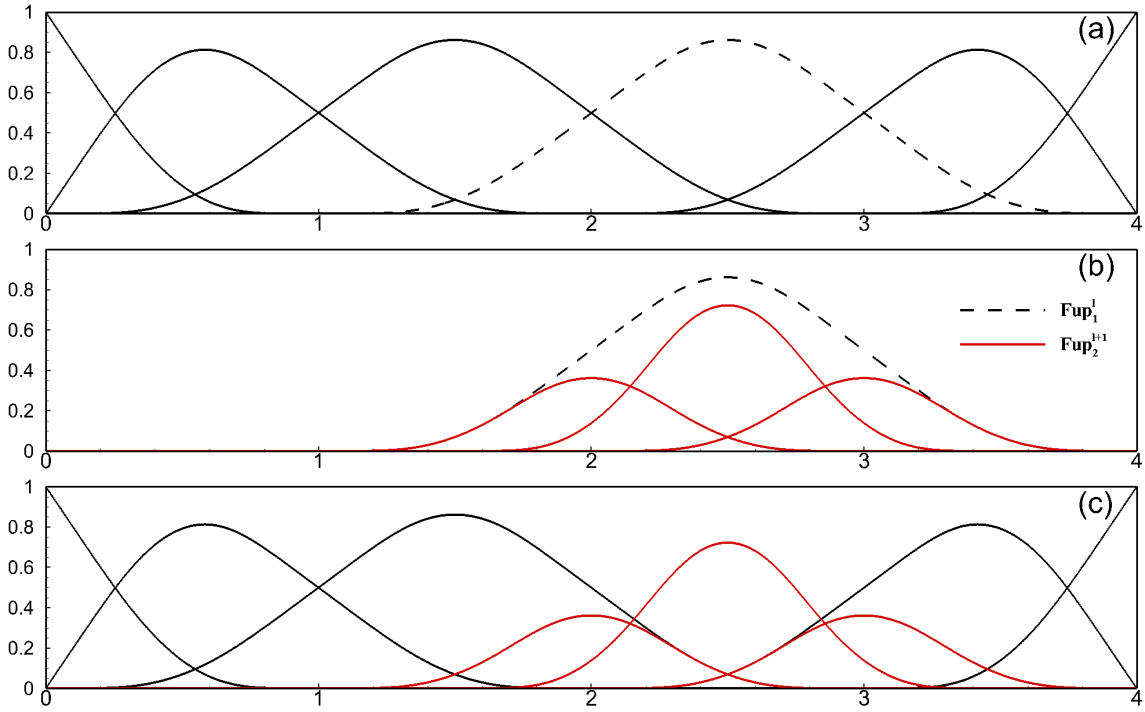

Figure 4: The three steps to construct hierarchical Fup basis functions. (a) In level l, basis functions $\mathcal{F}_p^l$ that need to be refined are determined (black dashed curve $|Fup_1^l$) and they are defined as *passive*, while remaining basis functions are defined as *active*; (b) In level $l+1$, three children (red solid curves $|Fup_2^{l+1}$) are designated as *active*; and (c) all *active* basis functions from levels l and $l+1$ are summed and form the hierarchical Fup basis functions $\mathcal{F}_{hbf}^{l+1}$.

3. Adaptive methodology

The 2-D adaptive spatial strategy used in this work is a novel approach based on the Control Volume IsoGeometric Analysis, shortly CV-IGA (Malenica *et al.* [46], [50], Gotovac *et al.* [16]) and hierarchical Fup basis functions (*hp*-refinement; see Kamber *et al.* [47]). Firstly, CV-IGA concept is explained. In the section 3.4, adaptive scheme for approximating known function is presented. It is used for easier understanding of whole adaptive process and serves as introduction for boundary value problems (BVPs). In the section 3.5, adaptive strategy for solving BVP with its differences, but also similarities with approximation of a known function is presented.

3.1. Control volume isogeometric analysis

In FEA there is one notion of a mesh and another for element, but also one element has two representations, one in the parent domain and one in physical space. Degrees of freedom of the finite elements are usually the values of the basis functions at the nodes, and elements

are usually defined by their nodal coordinates. Finite element basis functions, often referred to as "interpolation functions" or "shape functions", are typically interpolatory and may take on positive and negative values. However, for example in NURBS, the basis functions are usually not interpolatory and there are two notions of meshes, the control mesh and the physical mesh. The control points (see Figure 5) define the control mesh and the control mesh interpolates the control points. The control points enables the designer to create a wide range of desired objects, for instance, in the aviation or car industry. The control mesh consists of multilinear elements and does not conform to the actual geometry. Instead, it can be described like a scaffold, that controls the geometry. Control variables that defines the control mesh are the degrees of freedom that are located at the control points (red circles on the Figure 5).

The physical mesh, i.e., decomposition of the actual geometry, consists of two types of elements, the patch and the knot span (see Figure 5). The patch may be thought of as a macro-element or subdomain. While there are multiple patches in FEM (one element one patch) in IGA most geometries, for academic test cases, can be modeled with a single patch. Each patch has two representations, one in physical space and one in a parent domain. Patches in two-dimensional topologies are rectangles (see Figure 5), and in three dimensions are a cuboid in the parent domain representation. Patches can be decomposed into knot spans bounded by knots which are points, lines and surfaces in 1-D, 2-D, and 3-D topologies, respectively.

Figure 5 shows schematic illustration of IGA how one 2-D subdomain or patch is transformed from the parameter (virtual) space to the physical (real) space using following spline representation

$$x(\xi,\eta)=\sum_{j=1} x_j\phi_j(\xi,\eta); \quad y(\xi,\eta)=\sum_{j=1} y_j\phi_j(\xi,\eta) \tag{34}$$

where x_j and y_j are the coordinates of the control points $\mathbf{B}(x_j, y_j)$ in the physical space, while ξ and η represents the coordinates in the parameter space. However, the main part of (34) are spline basis functions ϕ_j which in classic IGA are B-splines and NURBS. It is clear from (34) that IGA operates only with basis functions in the parametric regular domain since transformations from the parametric to real physical space, and vice versa are defined by the Jacobian

$$J=\begin{bmatrix}\frac{\partial x}{\partial \xi} & \frac{\partial y}{\partial \xi}\\ \frac{\partial x}{\partial \eta} & \frac{\partial y}{\partial \eta}\end{bmatrix}=\sum_{j=1}^{N}\begin{bmatrix}\frac{\partial \phi_j}{\partial \xi}x_j & \frac{\partial \phi_j}{\partial \xi}y_j\\ \frac{\partial \phi_j}{\partial \eta}x_j & \frac{\partial \phi_j}{\partial \eta}y_j\end{bmatrix} \tag{35}$$

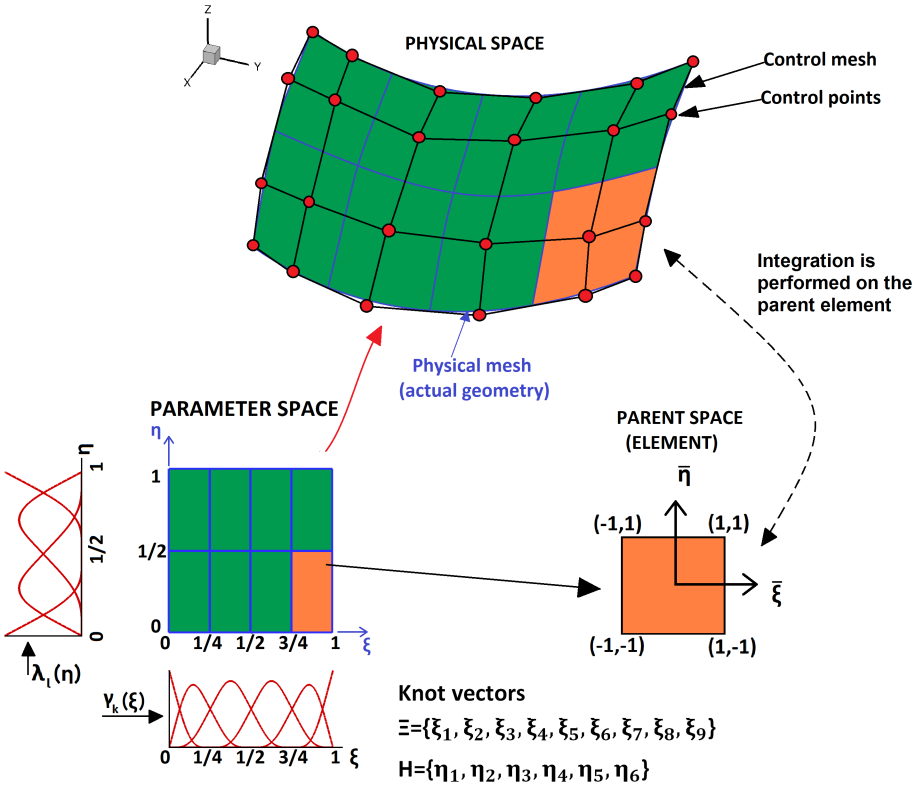

Figure 5: Schematic illustration of isogeometric analysis (IGA): physical space with control points and control mesh, parameter space with spline basis functions and related parent elements, knot vectors, and index space.

and its inverse

$$J^{-1} = \begin{bmatrix} \frac{\partial \xi}{\partial x} & \frac{\partial \eta}{\partial x} \\ \frac{\partial \xi}{\partial y} & \frac{\partial \eta}{\partial y} \end{bmatrix} = \frac{1}{\det J} \begin{bmatrix} \frac{\partial y}{\partial \eta} & -\frac{\partial y}{\partial \xi} \\ -\frac{\partial x}{\partial \eta} & \frac{\partial x}{\partial \xi} \end{bmatrix}, \tag{36}$$

as in classic FEM. However, the main difference is that IGA considers the transformation of each patch, which can be thought of as a macro-element or a subdomain, while the FEM performs transformations for each element [15].

The numerical solution in the parametric space is also described by independent set of spline basis functions

$$u(\xi, \eta) = \sum_{j=1} \alpha_j \varphi_j(\xi, \eta) \tag{37}$$

It should be noted that number and order of the basis functions in the (34) and (37) may not be the same.

In the following, the control volume discretization process will be presented by considering a simple steady-state advection-dispersion equation (ADE) in the form:

$$\nabla \cdot (D\nabla u(\mathbf{x})) - \nabla \cdot (vu(\mathbf{x})) = 0 \quad in \quad \Omega \tag{38}$$

with appropriate boundary conditions:

$$u(\mathbf{x}) = u_D \quad on \quad \Gamma_D \tag{39}$$

$$(D\nabla u(\mathbf{x}) - vu(\mathbf{x})) \cdot \mathbf{n} = q_N(\mathbf{x}) \quad on \quad \Gamma_N \tag{40}$$

where $u(\mathbf{x})$ represents the dependent variable, while the first and second term in Equation (38) represent influence of the dispersive (diffusive) and advective (convective) flux, respectively, which in general may be function of time, space and/or an unknown solution. Domain boundaries under the Dirichlet and Neumann boundary conditions are Γ_D and Γ_N, respectively, and $\mathbf{n}$ is the outward normal vector.

Method of weighted residuals can be thought as a general approach for deriving the different numerical formulations. The main idea is to integrate differential equation (38) over the domain of interest and multiply it by a finite number of weighting (test) functions $w_i(\mathbf{x})$:

$$\int_\Omega \nabla \cdot (D\nabla u(\mathbf{x}))w_i(\mathbf{x})d\Omega - \int_\Omega \nabla \cdot (vu(\mathbf{x}))w_i(\mathbf{x})d\Omega = 0 \tag{41}$$

where the number of test functions (w_i) is generally the same as the number of basis functions. Two most used formulations in IGA are Galerkin (G-IGA; test functions are the same as basis functions, Hughes *et al.* [12]) and collocation formulation (C-IGA; test functions are Dirac functions located at Greville points, Schillinger *et al.* [51]). However in this work, formulation of control volume within IGA (CV-IGA) will be introduced.

The control volume formulation is performed by firstly dividing the parametric space by m control volumes (see Figure 6) ($\Omega_i; i = 1, ..., m$). CV formulation [52] uses test functions defined in the following form:

$$w_i(x) = \begin{cases} 1 & \mathrm{x} \ \in \Omega_i \\ 0 & \mathrm{x} \notin \Omega_i \end{cases}, \Omega_i \in \Omega. \tag{42}$$

Substituting (42) in (41) and integrating only over the i-th control volume (CV) due to the properties of the test functions (42), the volume integrals at left side over the control volume are transformed into a surface integrals across Ω_i boundaries Γ_i using Gauss's theorem:

$$\int_{\Gamma_i} \big(D\nabla u(\mathbf{x})\big)\boldsymbol{n}d\Gamma - \int_{\Gamma_i} \big(vu(\mathbf{x})\big)\boldsymbol{n}d\Gamma = 0 \tag{43}$$

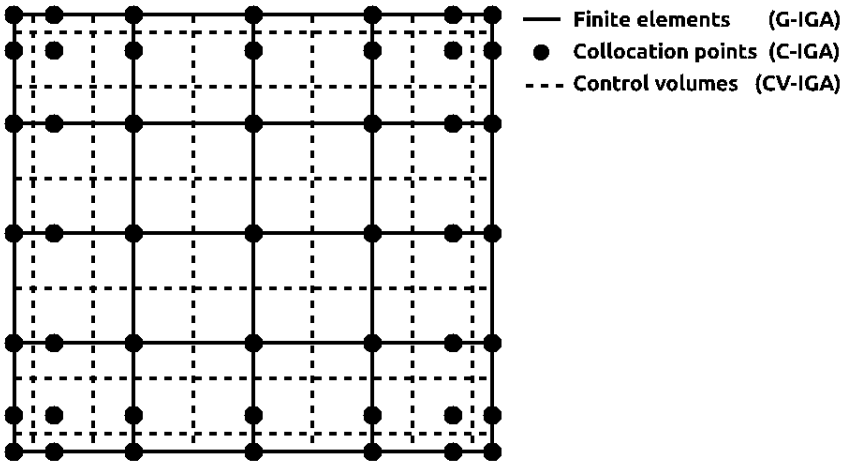

Figure 6: Discretization of 2-D domain with three different IGA formulations. Note that Greville points (black circles) represents collocation points but also locations of the vertices of basis functions which are crucial for creating CV boundaries.

where $\boldsymbol{n}$ is outward normal vector, thus obtaining the ADE conservative form.

Finally, weak formulation (43) is defined on each control volume using spline basis functions and unit compactly supported test functions (42) in order to get fully discretized control volume formulation:

$$\alpha_j \left[\int_{\Gamma_i} \big(D\nabla\varphi_j(\mathbf{x})\big)\boldsymbol{n}d\Gamma_i - \int_{\Gamma_i} \big(v\varphi_j(\mathbf{x})\big)\boldsymbol{n}d\Gamma_i \right] = \int_{\Gamma_{N_i}} q_N d\Gamma_N \tag{44}$$

where i denotes index of control volume and row of stiffness/conductance matrix, while j denotes index of spline basis function and column of the stiffness/conductance matrix. It is valid for all internal CV faces and boundary CV faces with Neumann boundary conditions. This implies that Neumann boundary conditions are weakly imposed by incorporating the known value of q_N to the weak formulation. However, as in G-IGA, Dirichlet essential boundary conditions requires special treatment. In this paper, Dirichlet boundary conditions are satisfied in the strong sense by directly satisfying the boundary conditions values in the following form:

$$\int_{\Gamma_{D_i}} u(\mathbf{x})d\Gamma_{D_i} = \int_{\Gamma_{D_i}} u_D(\mathbf{x})d\Gamma_{D_i} \tag{45}$$

After using set of spline basis functions for representation of the numerical solution $u(\mathbf{x})$

(see Eq. (37)) yields

$$\alpha_j \int_{\Gamma_{D_i}} \varphi_j(\mathbf{x}) d\Gamma_D = \int_{\Gamma_{D_i}} u_D(\mathbf{x}) d\Gamma_D. \tag{46}$$

It should be noted that Dirichlet boundary conditions are satisfied in similar sense as in classical FEM. Equations linked with CVs which contain Dirichlet boundary conditions are replaced with (45), and later when we solve the system of equations and get unknown spline coefficients, from these memorized equations the Dirichlet boundary fluxes are calculated.

Conservation is an interesting feature of the control volume formulation. The conservation is exactly satisfied over any control volume (local conservation), as well as over the whole computational domain (global conservation). Furthermore, even the coarse-mesh solution exhibits an exact integral balance [52].

CV-IGA requires cheaper numerical integrations then G-IGA because control volume formulation (43) requires only integration over CV boundaries Γ_i, while Galerkin formulation requires (full) integration over the part of domain where the particular test function is defined. Furthermore, the number of nonzero basis functions for each discretized equation in CV-IGA is lower then in G-IGA, thus the cost for the solution of the system of equations is generally lower then that for G-IGA. For comparison, the number of nonzero basis functions for CV-IGA for each discretized equation is $(n+2)^{dim}$ for odd order of basis functions and $(n+3)^{dim}$ for even, whereas for G-IGA this number is defined by $(2n+3)^{dim}$, where dim denotes the dimensionality of the problem. On the other side, CV-IGA is more expensive than C-IGA which contains only one integration (collocation) point per degree of freedom and smaller number of nonzero elements in the stiffness/conductance matrix. Generally, CV-IGA lies between two classical IGA formulations enabling local and global mass conservation (see details in Gotovac *et al.* [16]).

3.2. 2-D basis functions

Multi-dimensional Fup basis functions are obtained as tensor products of the one-dimensional basis functions defined for each coordinate direction. For example, the two-dimensional Fup basis functions are defined as,

$$Fup_n(\xi,\eta) = Fup_n(\xi) \cdot Fup_n(\eta) \tag{47}$$

where $Fup_n(\xi)$ and $Fup_n(\eta)$ are n-th order Fup basis functions that are defined in the ξ- and η- parametric directions, respectively. Figure 7 shows two-dimensional $\mathrm{Fup}_1(\xi,\eta)$ basis function and its first partial derivative.

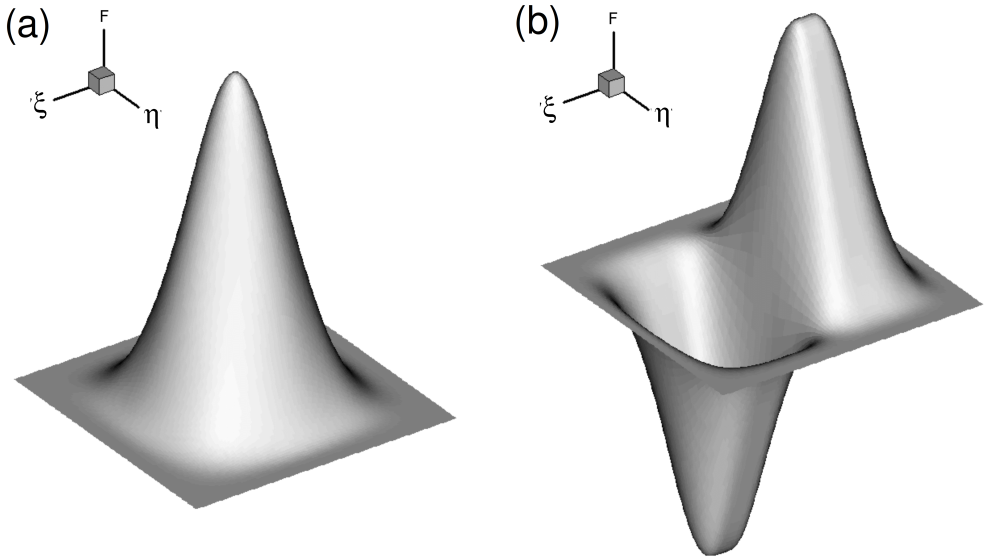

Figure 7: 2D Fup basis functions. F=Fup$_1(\xi,\eta)$; a)F and b)$\frac{\partial F}{\partial \xi}$.

For 1-D Fup basis functions, Fup$_n^l$ defined on Ξ^l can be represented as a linear combination of $n+2$ Fup$_{n+1}^{l+1}$ defined on Ξ^{l+1} (see Eq. (30)). Fup$_n^l(\xi,\eta)$ defined on the level l can be represented as a linear combination of $(n+2)$x$(n+2)$ i.e., $(n+2)^2$ Fup$_{n+1}^{l+1}$ defined on the level $l+1$,

$$Fup_n^l(\xi,\eta) = \sum_{i=0}^{n+1}\sum_{j=0}^{n+1} C_{n+1}^i C_{n+1}^j Fup_{n+1}^{l+1}\left(\xi - \frac{i}{2^{n+1}} + \frac{n+1}{2^{n+2}}\right) Fup_{n+1}^{l+1}\left(\eta - \frac{j}{2^{n+1}} + \frac{n+1}{2^{n+2}}\right) \tag{48}$$

where C_{n+1}^i and C_{n+1}^j are refinement coefficients (see Eq. (31)).

For example Fup$_1^l$ is defined on the knot vectors $\Xi^l = \{0, \frac{1}{3}, \frac{2}{3}, 1\}$ and $H^l = \{0, \frac{1}{3}, \frac{2}{3}, 1\}$, and its nine children Fup$_2^{l+1}$ (see Eq. (32)) are defined on a knot vectors $\Xi^{l+1} = \{0, \frac{1}{6}, \frac{1}{3}, \frac{1}{2}, \frac{2}{3}, \frac{5}{6}, 1\}$ and $H^{l+1} = \{0, \frac{1}{6}, \frac{1}{3}, \frac{1}{2}, \frac{2}{3}, \frac{5}{6}, 1\}$.

The trial function space of uniformly distributed Fup$_n(\xi,\eta)$ basis functions on the resolution level l and given order n are defined over the knot vectors in the form $\Xi = \{\xi_1, \xi_2, ..., \xi_{m^\xi}\}$ and $H = \{\eta_1, \eta_2, ..., \eta_{m^\eta}\}$, where m^ξ and m^η represents number of basis functions in ξ- and η- directions, respectively. The number of basis functions on the first resolution level $m^{l,\xi}, m^{l,\eta}; l = 0$ are defined as input parameters.

Length of the characteristic intervals $(\Delta\xi, \Delta\eta)$ are calculated as

$$\Delta\xi^l = \frac{\xi_{m^\xi+n+2} - \xi_1}{(m^{l,\xi} - n - 1)2^l}; \quad \Delta\eta^l = \frac{\eta_{m^\eta+n+2} - \eta_1}{(m^{l,\eta} - n - 1)2^l}, \tag{49}$$

where ξ_1 and $\xi_{m^\xi+n+2}$ are the first and last members of the knot vector in ξ- direction and η_1 and $\eta_{m^\eta+n+2}$ are the first and last members of the knot vector in η- direction on the first resolution level ($l = 0$).

Basis functions whose compact support is at least partially located outside the domain are modified by satisfying i-th derivations (see equation (28)). In the vector of mutually displaced Fup_n basis functions in 2-D, it is necessary to modify the $(n + 2)$ basis functions in ξ and/or η direction if they are near boundary of the domain.

3.3. Selection of control volumes

CV-IGA directly depends on selection of dimensions and positions of CVs. Since control volume approach can be considered as subdomain collocation, selection of control volumes is directly related to the Greville collocation points (see IGA collocation for example in Schillinger *et al.* [51]). The vertex of the basis function, i.e., the coordinate ξ_T, is the point with the maximum function value. The vertex serves as the origin for the shifting of the basis functions along the ξ and η axis by the length of the characteristic interval $(\Delta\xi, \Delta\eta)$. However, not all vertices are uniformly spaced according to the length of the characteristic interval. Vertices of the modified boundary basis functions (see subsection 2.2) are shifted and located inside the domain area. Their exact location can be calculated. In case of the B-splines of order n, the Greville points are defined to be the mean location of $n - 1$ consecutive knots in the knot vector for each basis spline function of order n [53]. Since Fup basis functions have one more characteristic interval for the same order, the grid points of the Greville abscissae calculated for the B_n correspond to the Greville abscissae grid points of the Fup_{n-1}. The Greville abscissa (Figure 6 - black circles) for the Fup_n basis functions can easily be computed from a knot vector $\Xi = \{\xi_1, \xi_2, ..., \xi_{m+n+2}\}$

$$\hat{\xi}_i = \frac{1}{n+1}(\xi_{i+1} + ... + \xi_{i+n+1}), \quad i = 1, ..., m \tag{50}$$

where n is the order of the basis functions, and m is the number of basis functions. From this point, when basis function vertex is mentioned, it is referred to the real coordinate of the vertex, except for modified boundary basis functions whose vertex coordinates are represented by the Greville points.

Figure 6 shows distribution of finite elements, collocation points and control volumes for all three IGA formulations (see also Gotovac *et al.* [16]). For each control volume (CV), there are four CV boundaries or faces. Each CV boundary represents side faces of CV in a manner that it lies in the middle between two adjacent Greville points (see also Figures 8

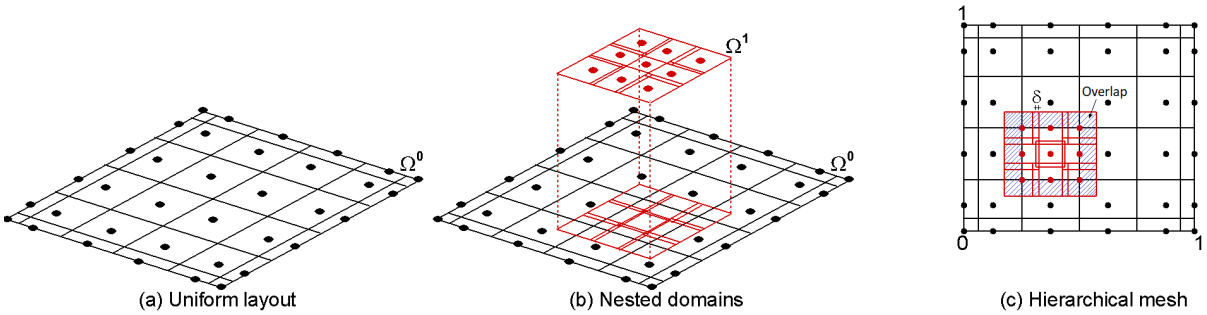

Figure 8: A nested sequence of CV domains for the construction of the Fup hierarchy according to relation $\Omega^l \supseteq \Omega^{l+1}$ for two-dimensional case. (a) uniform nonoverlapping CV distribution at the first level; (b) CV distribution on the first and second resolution level with active Fup basis functions from $\mathcal{F}^0$ and $\mathcal{F}^1$; (c) Hierarchical mesh with overlapping CVs (dots represents basis functions vertices).

and 9). Figure 8 shows a nested sequence of CVs domain, together with the corresponding vertices for each resolution level l, where each CV is linked with only one Greville point (vertex) i.e., the number of basis functions corresponds to the number of CVs.

Figure 8a) shows uniformly distributed Fup_1 basis functions on the knot vectors $\Xi^0 = \{0,0,0,\frac{1}{8},\frac{2}{8},\frac{3}{8},\frac{4}{8},\frac{5}{8},\frac{6}{8},\frac{7}{8},1,1,1\}$ and $H^0 = \{0,0,0,\frac{1}{8},\frac{2}{8},\frac{3}{8},\frac{4}{8},\frac{5}{8},\frac{6}{8},\frac{7}{8},1,1,1\}$ with the position of vertices (black dots) and corresponding CVs represented with solid line. Furthermore, after replacing one Fup_1 (assigned as passive) basis function from the first resolution level, nine Fup_2 basis functions (red dots, assigned as active) are introduced to the second resolution level (Ω^1). Each CVs boundary on the higher second level (see Figure 8b-c) are positioned exactly half the length of the characteristic intervals $\Delta\xi$, $\Delta\eta$ (see Eq. (49)) from the corresponding Fup basis function vertex, thus higher levels (CVs) are overlapping with lower levels (CVs). After assembling all active basis functions (assembles active Fup_1 and Fup_2 basis functions; $\mathcal{F}^1 = \mathcal{F}^0_a \cup \mathcal{F}^1_a$), CV overlapping distribution is defined for these two levels. However, it is possible that few CVs from higher level cover the same area as one larger CV from the lower level which creates problem of linearly dependent equations. Therefore, higher level that is in contact with lower level should have increased CV area to avoid problem of singular stiffness matrix. Enlargement of CV dimensions to $\Delta\xi(1+\delta)$, $\Delta\eta(1+\delta)$ can be chosen using parameter $\delta \in \langle 0, \frac{1}{2}\rangle$. Here, we choose $\delta = \frac{1}{4}$ (see Figure 8c). All Cvs from different resolution levels are rectangles in the parametric domain. Overlapping of some CVs makes this algorithm even more robust, but main advantage is easier process of constructing test (weight) functions in two-dimensional domains. Also, it should be emphasized that the

CV overlapping is the simplest possible algorithm when compiling hierarchical mesh and to simplify the numerical integration across each control volume. Some different algorithm could avoid overlapping of CVs, but would make integration process more complex over unregular CVs including cumbersome meshing procedure with Voronoi cells. We choose as simple as possible algorithm with all regular CVs in the parametric space, while avoiding any meshing procedure which can compromise meshless nature of CV-IGA.

3.4. Adaptive strategy for the function approximation

Adaptive CV-IGA with hierarchical Fup basis functions is easy and effective to present firstly in the simple functions approximation. The main idea is to represent the known function (f) in an adaptive manner so that coarse control volumes and lower order of Fup basis functions are used in regions where the solution is smooth, while fine control volumes and a higher order of Fup basis functions are used in those areas where the solution varies strongly.

The approximation $\tilde{f}(x,y)$ of the known function $f(x,y) : \Omega \to \mathbb{R}$ is presented in the form of the linear combination of Fup basis functions. The difference between the known function $f(x,y)$ and its numerical approximation $\tilde{f}(x,y)$ yields the numerical error:

$$\varepsilon(x,y) = f(x,y) - \tilde{f}(x,y) = f(x,y) - \sum_{j=1}^{m} \alpha_j \varphi_j(x,y) \tag{51}$$

The meaning of the approximation is to minimize the error $\varepsilon(x,y)$. If the control volume formulation is applied, the unknown coefficients α_j are obtained from the following system of equations:

$$\sum_{j=1}^{m} \alpha_j \int\limits_{\Omega_i} \varphi_j(x,y) d\Omega = \int\limits_{\Omega_i} f(x,y) d\Omega; \quad i,j = 1,2,...,m \tag{52}$$

which can be presented in a reduced matrix form:

$$a_{ij}\alpha_j = b_i; \quad i,j = 1,2,...,m \tag{53}$$

where

$$a_{ij} = \int\limits_{\Omega_i} \varphi_j(x,y) d\Omega; \quad b_i = \int\limits_{\Omega_i} f(x,y) d\Omega. \tag{54}$$

The adaptive criteria for the function approximation is defined as:

$$\int\limits_{\Omega_A} \frac{1}{\Omega_A} \left(|f(x,y) - \tilde{f}(x,y)| \right) d\Omega < \varepsilon_A \tag{55}$$

where ε_A represents the defined threshold and Ω_A is the integration area. Adaptive criteria (ε_A) defines whether Fup basis functions are kept or replaced while refining resolution level l. For the i-th control volume (CV), boundaries are defined via $\Gamma_{i,j,l}$,$\Gamma_{i,j,r}$,$\Gamma_{i,j,u}$ and $\Gamma_{i,j,d}$ (see Figure 9), where subscript letter l (left), r (right), u (up) and d (down) represents side faces of the CV. Since the numerical approximation ($\tilde{f}$) satisfies the average function value of the known function (f) over every CV_i ($i = 1, 2, ..., m$) on the current resolution level, the main problem for enabling an adaptation is to test how close the numerical approximation ($\tilde{f}$) is with respect to the known function (f). Therefore, we perform testing on the each quarter of the CV (see Figure 9). If all CVs satisfy adaptive criteria, the adaptive procedure stops. However, if one or more CVs did not satisfy Eq. (55), than those CVs are marked as refinable. Furthermore, all corresponding Fup basis functions that are at least partially located inside refinable CVs are marked as *passive*. Other Fup basis functions are marked as *active*, and they are kept in the next level. For the *passive* Fup basis functions, the algorithm introduces their children, as it is earlier explained (see Eq. (30)). In this way, using mentioned adaptive criteria on CV quarters, adaptive hierarchical grid is created using the hierarchical Fup basis functions with different resolutions and orders over the adaptive grid.

3.5. Boundary value problems

The adaptive spatial strategy used for the boundary value problem (BVP) is in some sense similar to the one used for function approximation. In the following, focus will be on the main differences between these two strategies. The major differences are adaptive criteria and adaptation of boundary conditions.

In the function approximation, a known function is approximated, while in BVP, we usually do not know the solution of the differential equation. The question is how to solve (approximate) the BVP. One of the possible approaches is shown considering the ADE (see Eq. (38)). In that case, solving ADE is reduced to the flux conservation over all CVs (see Eq. (44)). Since the CV formulation exactly satisfies Eq. (44) (i.e., the weak integral form of the conservation law) over each CV on the current resolution level, the adaptive criteria is used to check the conservation error for each quarter of the particular i-th CV (see Figure 9) ie., the adaptive criteria for the ADE problem is defined as

$$\alpha_j \left[\int_{\Gamma_i} \big(D\nabla\varphi_j(\mathbf{x})\big)\boldsymbol{n} d\Gamma_i - \int_{\Gamma_i} \big(v\varphi_j(\mathbf{x})\big)\boldsymbol{n} d\Gamma_i \right] - \int_{\Gamma_{N_i}} q_N d\Gamma_N < \varepsilon_A \tag{56}$$

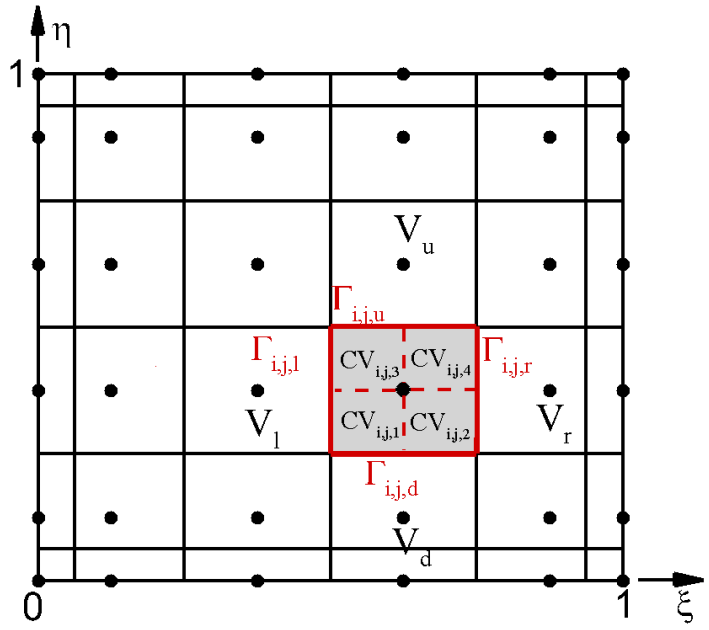

Figure 9: Dividing i-th CV into four equal parts ($\mathrm{CV}_{i,j,1}$, $\mathrm{CV}_{i,j,2}$, $\mathrm{CV}_{i,j,3}$ and $\mathrm{CV}_{i,j,4}$) while testing adaptive criteria on i-th CV.

where ε_A represents the defined threshold. All CVs where at least one of the quarters has the conservation error greater than the prescribed threshold are marked as refinable, and the adaptive procedure refines selected basis functions in the next level in the same way as for the function approximation. However, in BVP there are boundary conditions that needs to be satisfied. CVs with Neumann boundary conditions are satisfied in same sense as all internal CVs by checking conservation error for each quarter of the particular i-th CV, i.e. Neumann boundary conditions are weakly imposed by incorporating the known value (40) to the weak formulation (44). However, Dirichlet boundary conditions are satisfied in the strong sense by directly satisfying the boundary values (39). This implies that CVs with Dirichlet boundary conditions use calculated boundary fluxes from memorized equations and check mass conservation with other internal fluxes. If mass conservation is not satisfied, those Dirichlet CVs are marked as refinable.

In the function approximation, adaptive criteria is set to be related to the function accuracy Eq. (55), while in BVP the criteria is set to be the mass conservation error. However, the adaptive criteria can be defined in many ways. There are many other meaningful numerical and physical choices. For example, for function approximation, the function derivatives can be an ideal option in some cases. Furthermore, for BVP, the solution error between two

resolution levels can be defined as criteria [54]. Moreover, satisfaction of the Peclet number can be very valuable for ADE problems (see [55]). Finally, any combination of these criteria can also be new obtained criteria.

4. Numerical examples

4.1. Aim of the numerical examples

The aim of the numerical tests herein is to investigate whether adaptive refinement using hierarchical Fup basis functions achieves spectral convergence rates, even while solving problems that may involve singularities, contrary to the application of uniform grid.

Numerical examples are started with function approximation for easier understanding of whole adaptive process. This example demonstrates HF's ability to capture sharp fronts by introducing new levels into a portion of the domain where it is needed. To demonstrate the potential of HF within CV-IGA we address the following classical benchmark 2-D problems:

- Poisson equation
- Heat conduction problem
- Advection-dispersion problem

Analytical solutions are available for all problems except advection-dispersion problem. All of the examples illustrate the ability of HF's to efficiently and accurately describe different resolution scales.

4.2. Verification tests

4.2.1. Function approximation

The selected test 2-D function is:

$$f(x,y) = \arctan\left(50\left(-0.25 + \sqrt{x^2+y^2}\right)\right) \tag{57}$$

with chosen numerical parameters at the zero level $n = 1$, $m_x^0 = 10$, $m_y^0 = 10$ and the domain defined as $\Omega = [0,1]^2$. The error threshold is set as $\varepsilon_s = 10^{-7}$, which implies that the residual (see Eq. (51)) between the Fup approximation and the given function (57) over all CVs at all resolution levels must be less than this prescribed threshold. Figure 10 shows the evolution of the adaptive procedure using HF at five consecutive resolution levels starting with uniform $\mathrm{Fup}_1(x,y)$ basis functions.

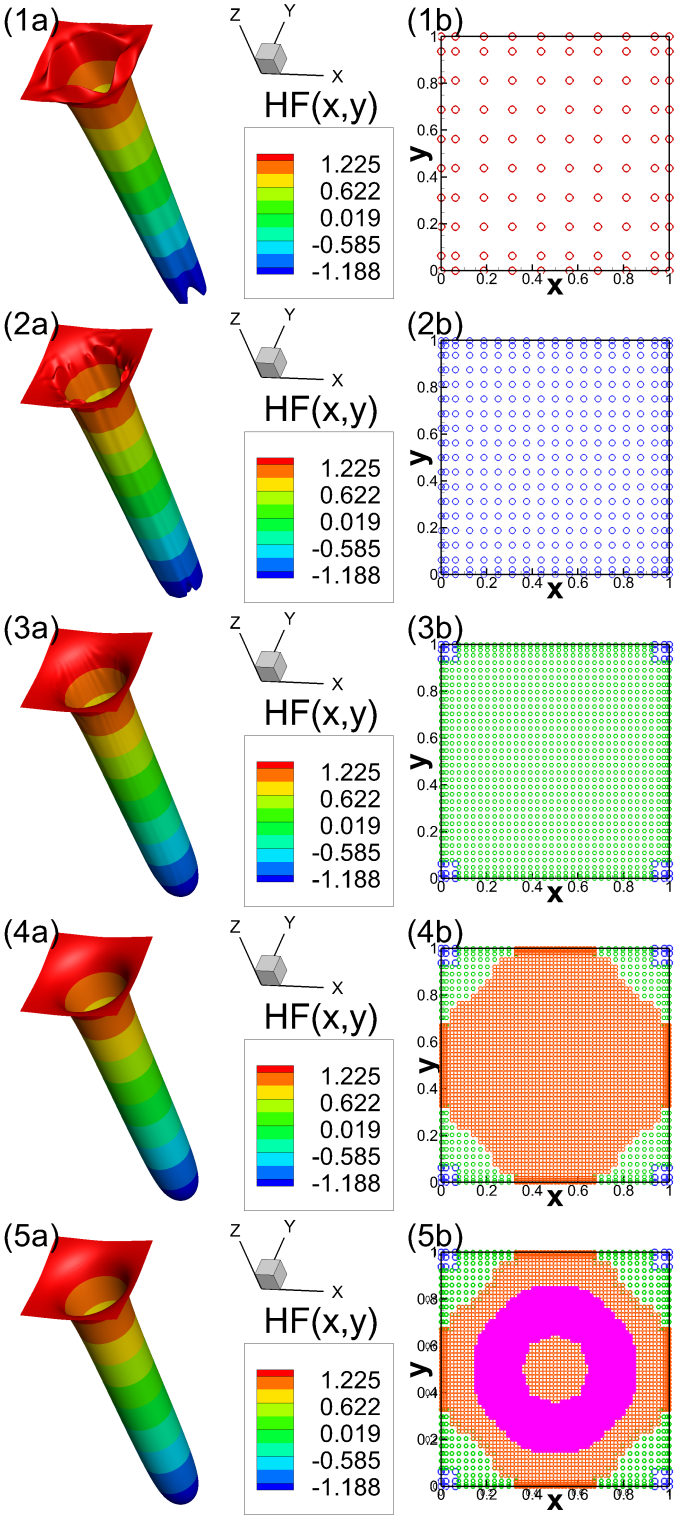

Figure 10: CV-IGA approximation of the function (57). (a) HF approximations of the given function, (b) the adaptive grid on different resolution levels where each color represents Fup basis function vertices on different level.

Function approximations of the given function (57) over all levels are shown in Figure 10(1a-5a). The error measure between the numerical approximation and given function is residual which can be calculated as the integral difference between those two functions on all quarters of the CVs. Figure 10(1b-5b) shows active basis functions used for the numerical approximation and are represented by their vertices (each color represents one level, i.e., active basis functions on that level). CVs are not directly shown but can be visualized with the help of the basis functions vertices, since every CVs edge is placed between the vertices of the adjacent functions (see Figure 8).

The adaptive procedure is repeated until all residuals are less then the prescribed threshold. For given function (57) and adaptive threshold set as $\varepsilon_s = 10^{-7}$, adaptive procedure needs five levels to approximate given problem, as shown in Figure 10. Note that fine CVs with a higher order of Fup basis functions are obtained only around the "well" edges describing high solution frequencies. Moreover, in other regions the adaptive grid uses lower order of Fup basis functions and coarse CVs which helps in reducing the computational cost and increases efficiency.

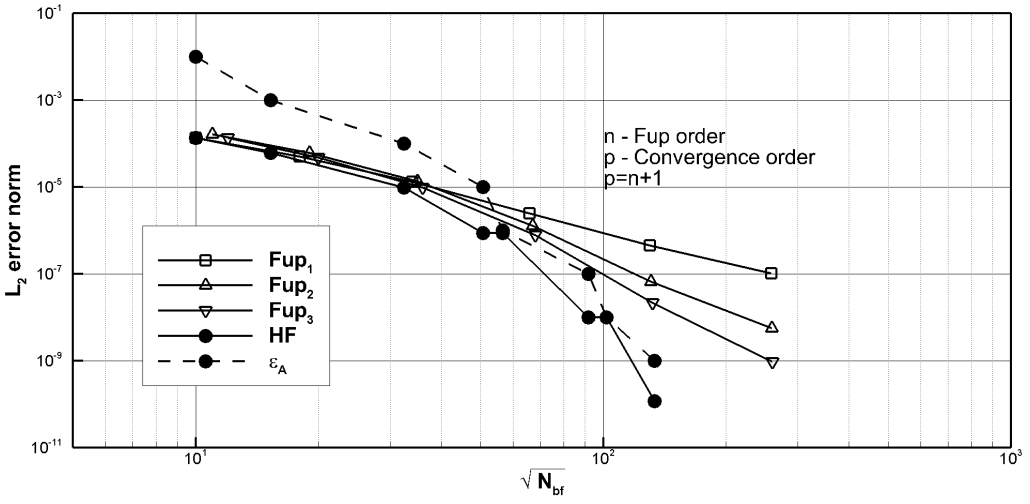

Figure 11: Convergence analysis obtained with uniform and adaptive Fup_n basis functions for the function approximation.

Figure 11 shows efficiency in terms of the L_2 error norm as a function of the total degrees of freedom (DOFs) with slope representing the convergence rate (p) confirming that $p = n + 1$ is valid for uniform grid if n is the Fup order. Adaptive procedure just like in one-dimensional case [47] yields spectral convergence (solid line with filled circles), contrary to the THB splines which ensures polynomial convergence ($p = n+1$). Spectral convergence

enables that convergence rate is higher than $p = n+1$ if n is the Fup order used at the highest resolution level. Spectral convergence is achieved due to using *hp*-refinement when higher resolution levels not only use basis functions with smaller scales or higher frequencies, but also increased order of basis functions. This *hp* property causes that new levels and DOFs more drastically increase accuracy than it is case with THB splines where all levels use the same order of the basis functions. Figure 11 shows that convergence plot have larger slopes when new resolution levels and increased order of basis functions are introduced. Furthermore, adaptive procedure achieves a higher accuracy then the prescribed threshold (dashed line with empty circles, ε_A), thus proving the control of the numerical error. This means that the real numerical error of the function approximation is strictly less than the prescribed threshold.

4.2.2. Poisson equation

For 2-D Poissson benchmark problem, so called wavefront well problem is considered. It is commonly used example for testing adaptive refinement algorithms because of a steep wave front in the interior of the domain [7, 56, 57]. Parameters determine the steepness and location of the wave front. With the arctangent wave front that has exact solution that is similar to the function (57), there is a mild singularity at the center of the circle. However, for this test center of the circle is outside the domain, thus performance on the wave front is examined, not the singularity.

Problem is defined in the form

$$\nabla \cdot (-\kappa \nabla u(x,y)) = f(x,y), \quad (x,y) \in \Omega \tag{58}$$

with boundary conditions

$$u(x,y) = u_D(x,y), \quad (x,y) \in \partial\Omega \tag{59}$$

The numerical simulation domain is defined by a square area $\Omega = [0,1]x[0,1]$ where the boundaries are $\Gamma_D = \partial\Omega$ and $\Gamma_N = \emptyset$ (see Figure 12a). The exact analytical solution for the pressure field is given by:

$$u(x,y) = \arctan\left(\alpha\left(r - r_0\right)\right) \quad \text{where} \quad r = \sqrt{(x-x_c)^2 + (y-y_c)^2} \tag{60}$$

where x_c and y_c represent center of the circular wave front, r_0 is the distance from the wave front to the center of the circle, and α gives the steepness of the wave front.

It should be noted that the right hand side $f(x,y)$ is generated by taking the Laplacian (∇^2) of the exact solution given in Equation (60). The exact solution depicted in Figure

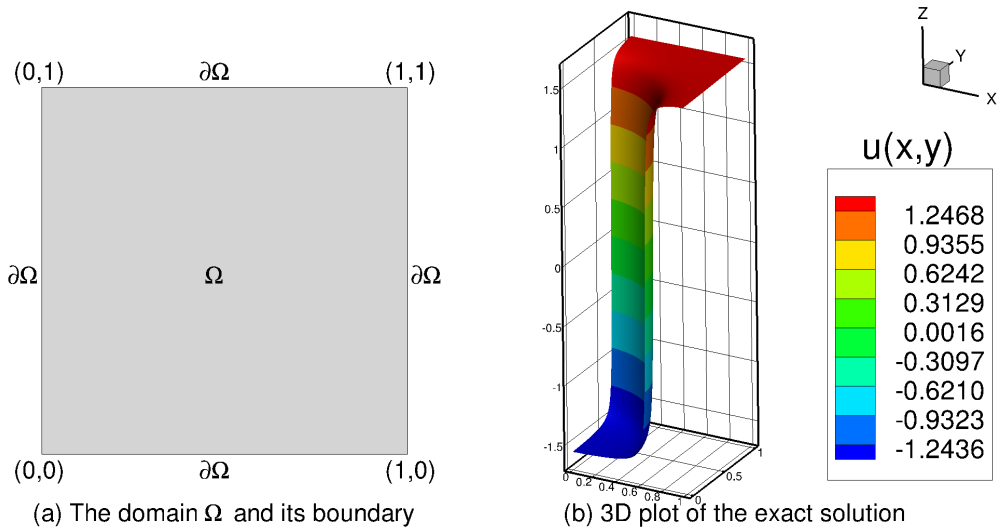

Figure 12: Numerical solution domain and exact solution plot of the wave well problem defined by Eq. (58).

12b displays a "front"-type of behavior where the solution is rapidly changing across a circular band (a quarter of a circle) inside the domain. For the conductivity matrix κ only isotropic case is considered, and for simplicity in deriving the source function, the conductivity equivalent coefficient is set equal to

$$\kappa = \begin{bmatrix} 1 & 0 \\ 0 & 1 \end{bmatrix} \tag{61}$$

The adaptive simulation shown in Figures 13 and 14 is performed with starting polynomial degree $n = 1$. Number of basis functions on uniform level is defined as $m_x^0 = 18$, $m_y^0 = 18$, center of circular wave front is set at $x_c = y_c = -0.05$ with $r_0 = 0.7$ and $\alpha = 100$. The error threshold is set as $\varepsilon_s = 1 \cdot 10^{-4}$, which implies that the mass conservation error over all quarters CVs on every level must be less than this prescribed threshold.

Figures 13 presents the absolute difference between the numerical and exact (see (60)) solution while Figure 14 presents the adaptive grid on different resolution levels. With every new level, numerical solution becomes closer to the real solution (Figure 13 1a-6a). Even though, difference between numerical solution and exact solution is presented in Figure 13 because exact solution is known, it was not the adaptive criteria used for testing like in approximating function (57). Here, adaptive criteria is used to check conservation error for each quarters of the particular i-th CV on the current resolution level. Quarters of the CVs are used because CV formulation exactly satisfies governing equation (i.e., the weak integral form of the conservation law), over each CV on the current resolution level. The adaptive

grid captures the front (see Figure 14) and repeats adaptive procedure until conservation error is less then the prescribed threshold at each quarter of the CVs. For given parameters and using HF, six levels are needed in order to find numerical solution that has conservation error less then prescribed error threshold on all quarters of the CVs.

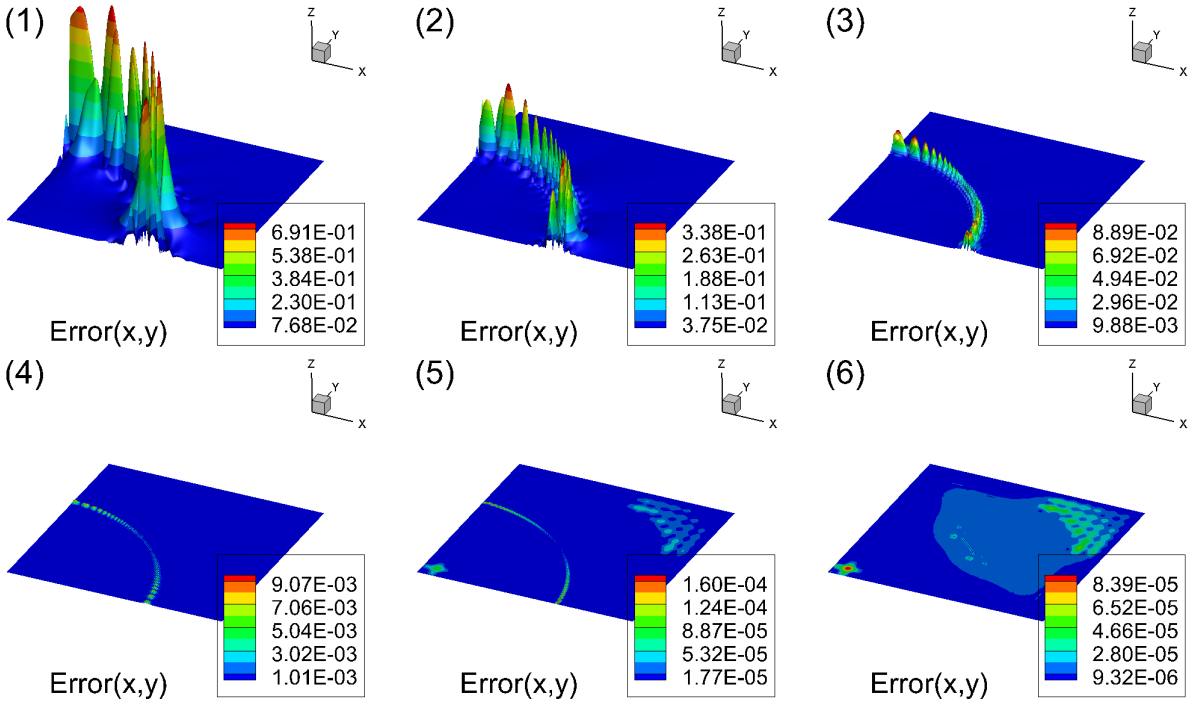

Figure 13: The absolute difference between the numerical and exact (60) solution on different resolution levels (1-6).

The convergence analysis for the uniform and adaptive procedure is shown in Figure 15. It depicts a demonstration of the efficiency in the terms of the L_2 error norm as a function of DOF, and shows that the convergence rate for CV-IGA using the uniform grid is the optimal ($p = n + 1$) for odd and the suboptimal ($p = n$) for even order (n) of basis functions. G-IGA (Galerkin) yields the optimal convergence rate for the Poisson problem for all orders of Fup basis functions (i.e., $p = n+1$), while C-IGA (collocation) yields suboptimal convergence rates of $p = n - 1$ for odd basis functions and $p = n$ for even basis functions [50, 16]. The adaptive procedure for this diffusive-like boundary value problem exhibits spectral convergence (black solid line with filled triangles), just like in one-dimensional case [47].

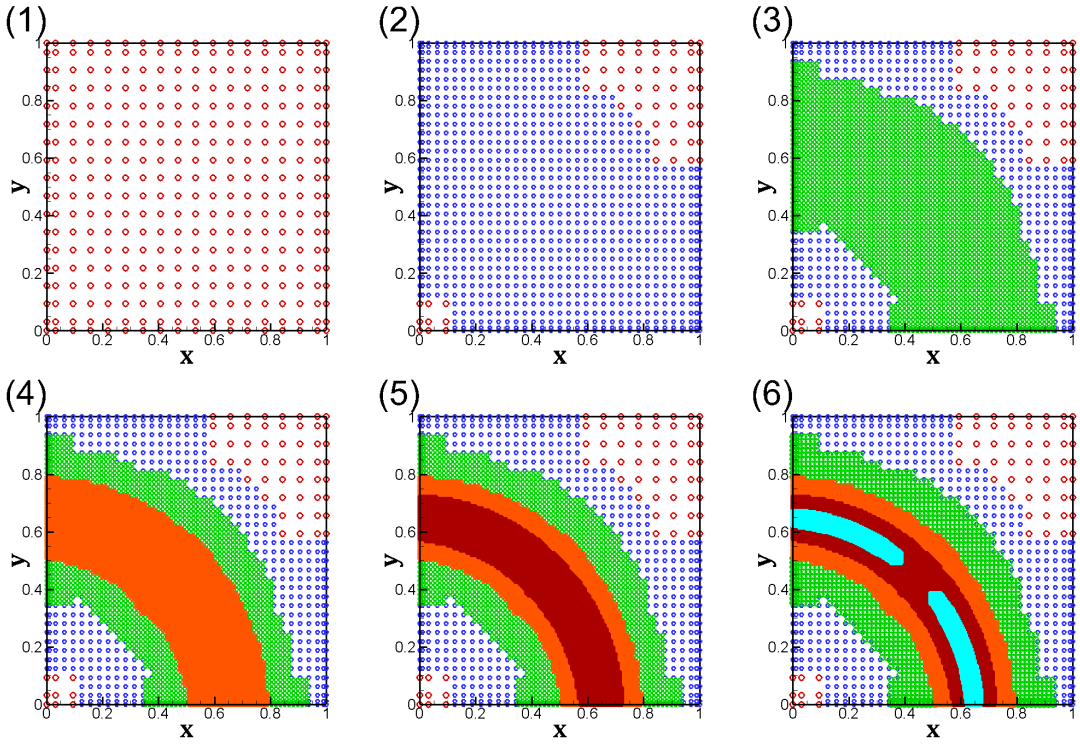

Figure 14: The adaptive grid on different resolution levels, (1) first, (2) second, ..., (6) sixth level. Each color represents Fup basis function vertices on different level.

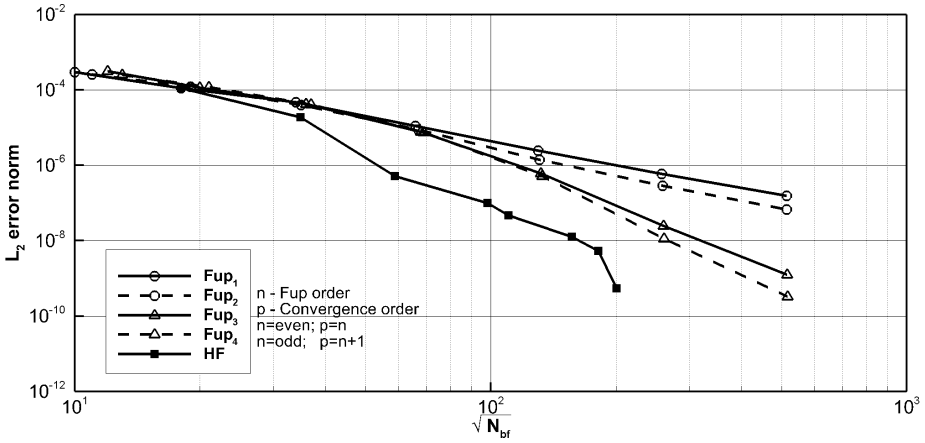

Figure 15: Convergence analysis of the wave front problem given in the form (58) for the uniform and adaptive procedure.

4.2.3. Heat equation (Laplace)

In this part, results obtained with adaptive algorithm on problems with irregular geometry are presented. Considering stationary heat conduction problem

$$\Delta u = 0 \tag{62}$$

on an L-shaped domain $\Omega = [-1,1]^2 \setminus [0,1]^2$, see Figure 16a), with boundary conditions

$$u = 0 \quad on \quad \Gamma_D \tag{63}$$

$$\frac{\partial u}{\partial n} = q_N \quad on \quad \Gamma_N \tag{64}$$

such that the exact solution is given by

$$u = r^{2/3} \sin\left(\frac{2\theta - \pi}{3}\right) \tag{65}$$

in polar coordinates (r, θ), where $r^2 = x^2 + y^2$ and $\theta = \arctan(y/x)$. The expression for the Neumann boundary condition q_N is derived based on the exact solution (65). For the given elliptic problem, the re-entrant corner at $(0,0)$ in the domain causes a singularity in the solution. An optimal convergence rate is not obtained when uniform mesh refinement is performed for the problems where the solution is not sufficiently smooth [21].

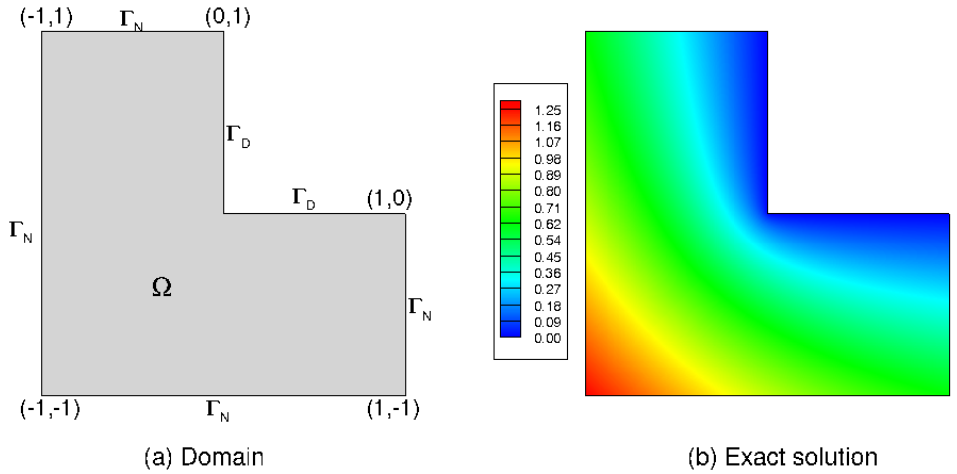

Figure 16: The L-shape problem: a) Numerical solution domain with boundary conditions and b) exact solution plot.

Presented HF procedure starts with $m_x^0 = 18$, $m_y^0 = 18$ Fup basis functions on the first (uniform) resolution level. The error threshold is set as $\varepsilon_s = 9 \cdot 10^{-3}$, which implies that the

mass conservation error over all quarters CVs on every level must be less then this prescribed threshold. The exact solution of the presented problem is shown in Figure 16b.

L-shaped domain is discretized by two patches, as shown in Figure 17b, while Figure 17a shows control points for the coarse mesh.

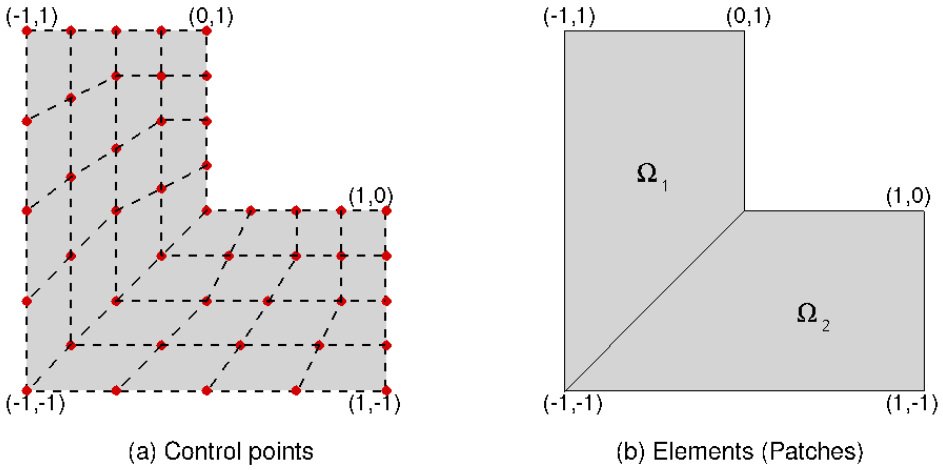

Figure 17: The L-shape problem: a) Fup discretized geometry with a $n_{cp} = 25$ number of control points per each element, and b) for $n_{el} = 2$ number of patches. In a) red circles represent the control points, whereas the shaded region is the modeled geometry.

Figure 18 presents the numerical solution for the stationary heat conduction problem in two-dimensional domain. The area of interest is detected and resolved locally using HF basis functions (see Figure 18). Refinement captures the re-entrant corner in the domain at $(0, 0)$ where a singularity in the solution occurs. For given parameters and using HF, six levels are needed in order to find numerical solution that has conservation error less then prescribed error threshold on all quarters of the CVs.

The convergence analysis is performed using L_2 norm and is plotted in Figure 19 for uniform Fup_1, Fup_2 and HF basis functions. It can be observed that adaptive HF basis functions again improves the convergence rate in comparison to the uniform layout. Moreover, uniform grids shows a significantly reduced convergence rate ($p = 0.3$) due to the re-entrant corner at $(0, 0)$ in the domain (singularity). The present numerical example thus confirms that adaptive algorithm significantly improves solution for rough problems still enabling spectral convergence. Convergence rate by parts is equal to unifom grid if new levels are not introduced. When new levels are introduced around singular corner, convergence rate exhibits spectral character. Overall, convergence is still spectral due to *hp*-refinement properties of the proposed method.

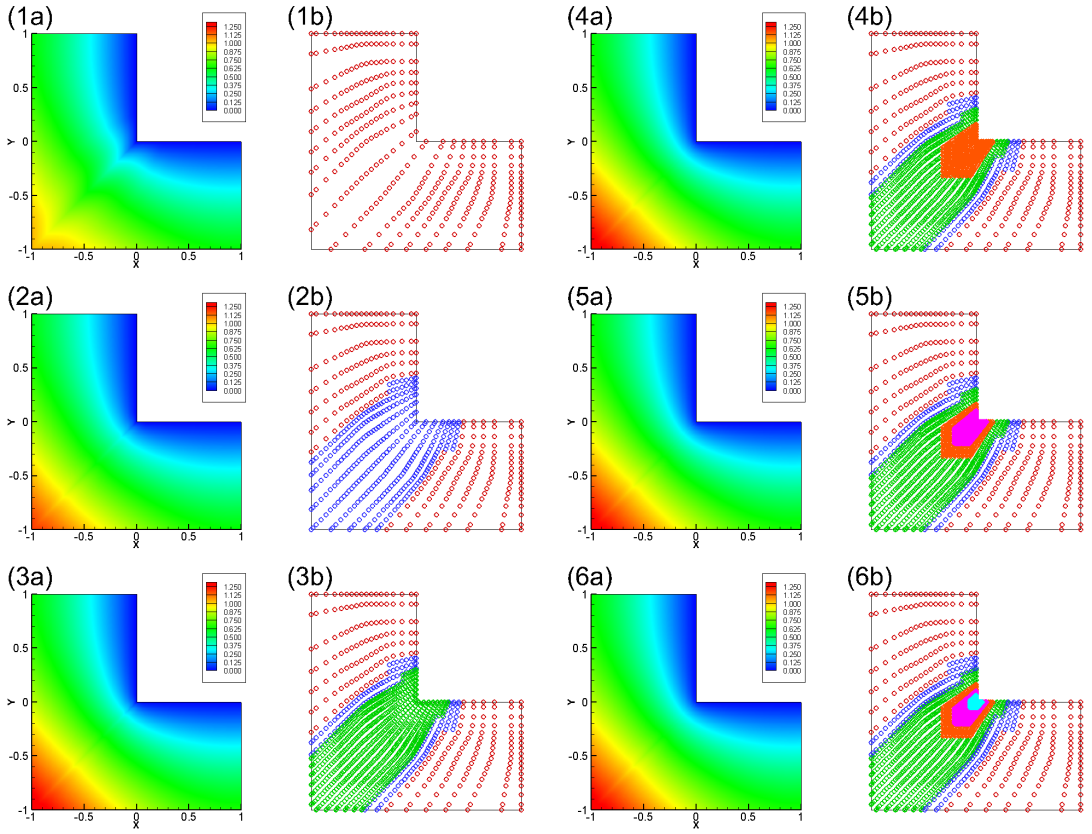

Figure 18: Numerical solution of the stationary heat conduction problem defined over an L-shaped domain (governed by Laplace equation (62)) at different resolution levels; (1a-6a) HF approximations; (1b-6b) corresponding adaptive spatial grids.

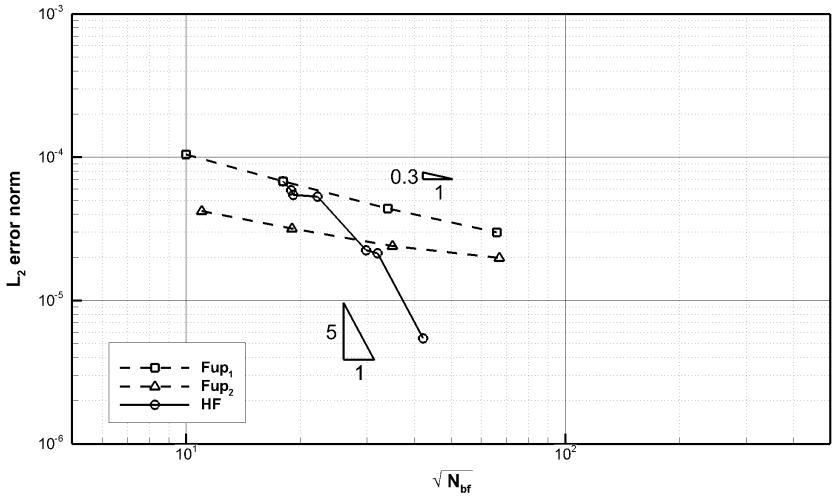

Figure 19: Convergence analysis for uniform and adaptive method for the L-shape problem.

4.2.4. Advection-dispersion equation

Steady-state discontinuous example

Two-dimensional benchmark example is taken from [12, 15, 23] which consists of solving the advection-dispersion equation

$$D\Delta u - v \cdot \nabla u = 0 \tag{66}$$

on the unit-square with discontinuous Dirichlet boundary conditions (see Figure 20). The dispersion D coefficient is chosen extremely small ($D = 8 \cdot 10^{-4}$) compared to the advection velocity $v = (\sin\theta, \cos\theta)^T$, thus very sharp layers are considered. Sharp interior and boundary layers require stable numerical techniques as well as adaptive solutions in order to capture all resolution scales. Adaptation with hierarchical Fup basis functions (*hp*-refinement) gives very accurate numerical results, but still needs large number of basis functions (unlike uniform basis layout), so SUPG stabilization [58] is employed as additional mechanism inside the adaptive procedure.

Adaptive resolution of the internal and boundary layers are investigated with the presented HF procedure starting from $m_x^0 = 18$, $m_y^0 = 18$ Fup basis functions on the first (uniform) resolution level. The error threshold is set as $\varepsilon_s = 1 \cdot 10^{-4}$. The exact solution of the presented problem is not known.

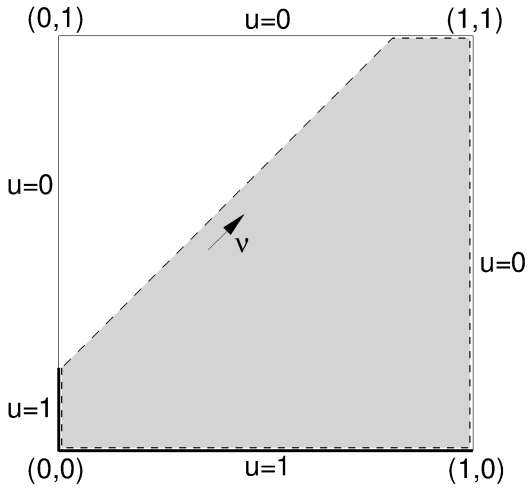

Figure 20: Domain with discontinuous Dirichlet boundary conditions for the Advection-dispersion problem.

Firstly, Figure 21 presents the evolution of the sharp boundary layer and corresponding adaptive spatial grids at five consecutive resolution levels in two-dimensional domain

without stabilization. It can be observed that the refinement captures the location of the internal and the boundary layers very well. Despite the high Peclet number no stability or robustness issues in the adaptive algorithm were encountered. There are some under- and overshooting of the first (uniform) level along the internal layer. These nonphysical oscillations are a result of the discretization of the first order spatial derivative in the advective term when this term dominates the other terms in the governing equation. Moreover, five adaptive HF refinement levels are required to get control over the undershooting close to the jump at the inflow boundary. Mass conservation error detects the internal layer as well as the boundary layer. However, the refined levels are not placed only around the boundary layer and the internal layer, solely because adaptive algorithm just like in one-dimensional case [47] requires stabilization process to efficiently solve this advection dominated problem (see Figure 22). It is more relevant to apply stabilization only to the first few levels (in this case, for the first three levels, $l = 1, 2, 3$) because the Peclet number is higher at the initial resolution levels. Figure 22 presents the evolution of the numerical solution and corresponding adaptive spatial grids at four consecutive resolution levels with the stabilization method applied to the adaptive algorithm. Comparing grids with (Figure 22) and without (Figure 21) stabilization, methodology which uses stabilization yields significant improvement. Moreover, the computational cost is reduced since fewer basis functions are needed on higher levels to achieve the same mass conservation error on all quarters of the CVs.

Figure 23 presents the convergence analysis of the adaptive algorithm using HF basis functions, with respect to the degrees of freedom used to achieve a certain accuracy. Since previous problem had reduced convergence rate for uniform test due to the singularity, in this test we skipped uniform analysis since problem has discontinuity within Dirichlet boundary conditions. As expected, HF adaptive algorithm achieves spectral convergence rate which is quite impressive for these type of problems. Note that previous authors did not present convergence plot for this ADE benchmark using THB.

Space-time advection-dispersion problem

This section describes the mixing of transport processes in the space-time domain, for instance in porous media [54]. Advection-dispersion process can be described by the following equation, in the form:

$$\frac{\partial C(x,t)}{\partial t} = D\frac{\partial^2 C(x,t)}{\partial x^2} - v\frac{\partial C(x,t)}{\partial x} \tag{67}$$

with appropriate initial and boundary conditions:

$$C(x,0) = 0 \tag{68}$$

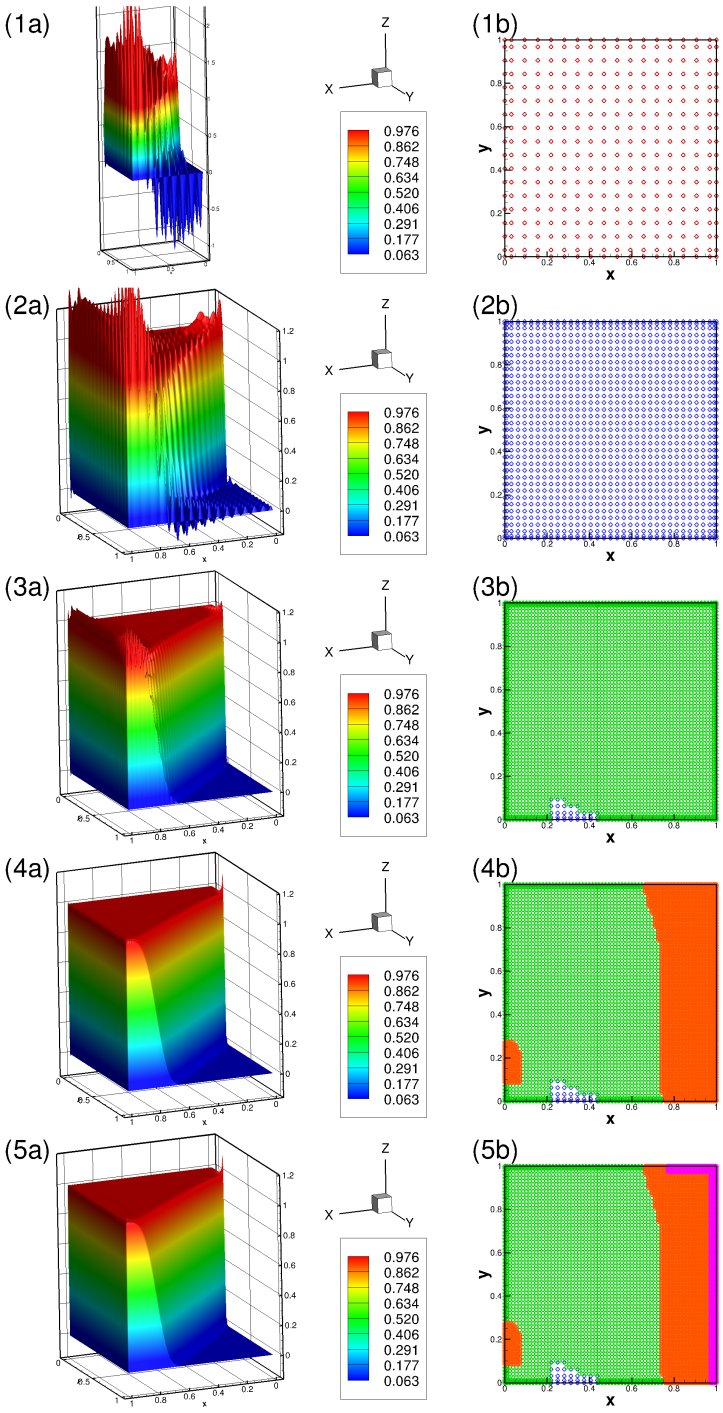

Figure 21: Numerical solution of the ADE (66) at different resolution levels (without stabilization); (1a-5a) HF approximations; (1b-5b) corresponding adaptive spatial grids.

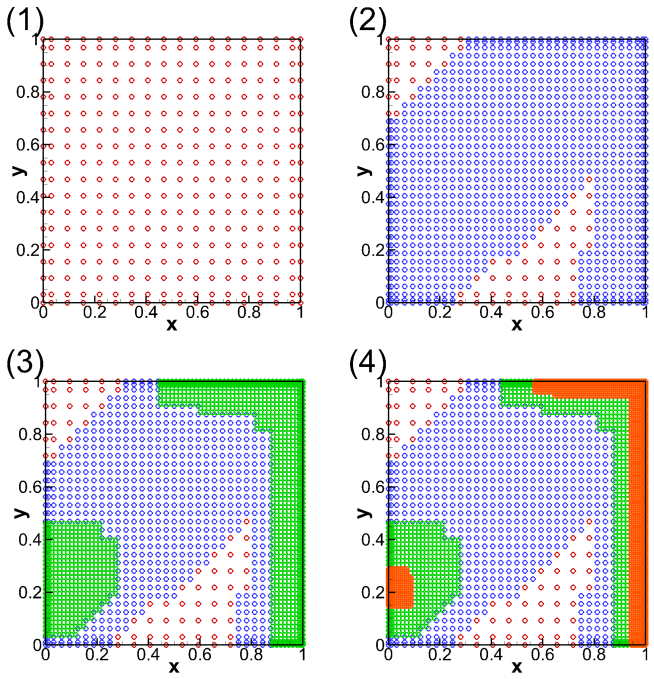

Figure 22: Numerical solution of the ADE (66) with stabilization procedure at different resolution levels: corresponding adaptive spatial grids at the (1) first, (2) second, (3) third and (4) fourth level.

$$C(0,t) = C_0; \quad \frac{\partial C(2,t)}{\partial x} = 0 \tag{69}$$

where C represents the dependent variable (concentration $[M/L^3]$), while D is the dispersion coefficient and v is the transport velocity in the x direction.

The domain, dispersion, velocity and threshold are defined by: $L = 2m$; $D = 10^{-5}$, $v = 10^{-3}$, $\varepsilon = 5 \cdot 10^{-4}$. The initial condition (see Eq. (68)) shows that initially the domain was occupied by fresh water ($C = 0$). However, the left boundary consists of denser fluid (for example the salt source) that continuously flows into the domain, and the right boundary states that there is no dispersion flux through that boundary.

Figure 24a shows the numerical solution in the x-t domain obtained with space-time HF basis functions. It represents the change in the solute concentration over the space and time. This change occurs in a narrow transition zone (see Figure 24). Figure 24b shows an adaptive grids in the space-time domain. In initial stages of the process, a fine CVs with higher order of Fup basis functions are needed due to very challenging initial conditions and the creation of a very sharp discontinuous concentration front. It should be noted that time domain is considered as one global time step. Furthermore, the initial error does not propagate

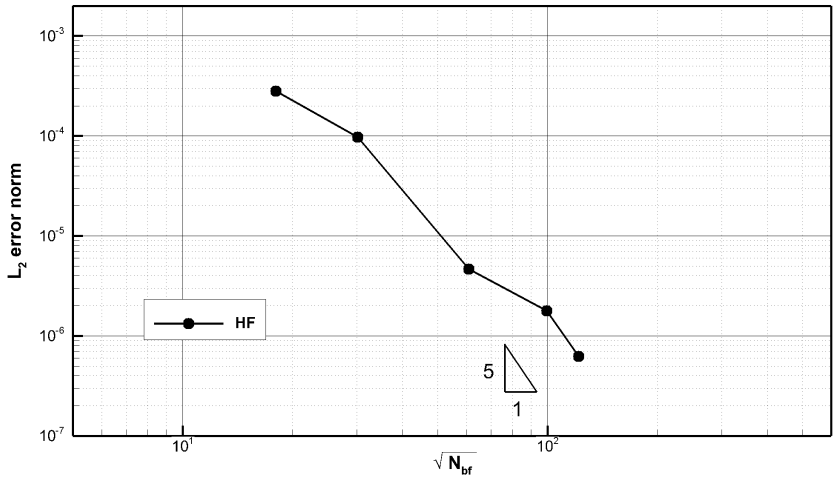

Figure 23: Convergence analysis for adaptive method of steady state advection dispersion problem (66).

further over time because proposed adaptive method converts the boundary-initial problem to a quasi-boundary problem controlling the global temporal/spatial error.

Figure 25 presents corresponding adaptive spatial grids at four consecutive resolution levels with the stabilization method. For two-dimensional cases, the idea of implementing stabilization method of upwinding can not be easily applied. Various methods have been proposed to implement the basic idea of upwinding to 2-D analyses. Here, upwinding method adjusting for 2-D analyses with control volume procedure is used [59]. Moreover, the computational cost is reduced since fewer basis functions and levels (Figure 24 vs Figure 25) are needed to achieve the same mass conservation error on all quarters of the CVs.

Figure 26 shows convergence analysis using L_2 norm. Uniform analysis is skipped since presented problem has singularity due to discontinuity of boundary conditions, thus only adaptive algorithm without stabilization is tested. It can be observed that adaptive HF basis functions achieves spectral convergence rate. This example is used to show how adaptive grid handles moving fronts and have the ability to change the grid dynamically, following a front during the simulation while keeping the spectral convergence rate.

5. Conclusions

This paper presents the development of new 2-D hierarchical Fup (HF) basis functions that enable local hp-improvement inside adaptive control volume isogeometric analysis (CV-IGA). HF provides spectral convergence and presents a substantial improvement in comparison to THB that enable polynomial convergence. Hierarchical Fup basis functions do not

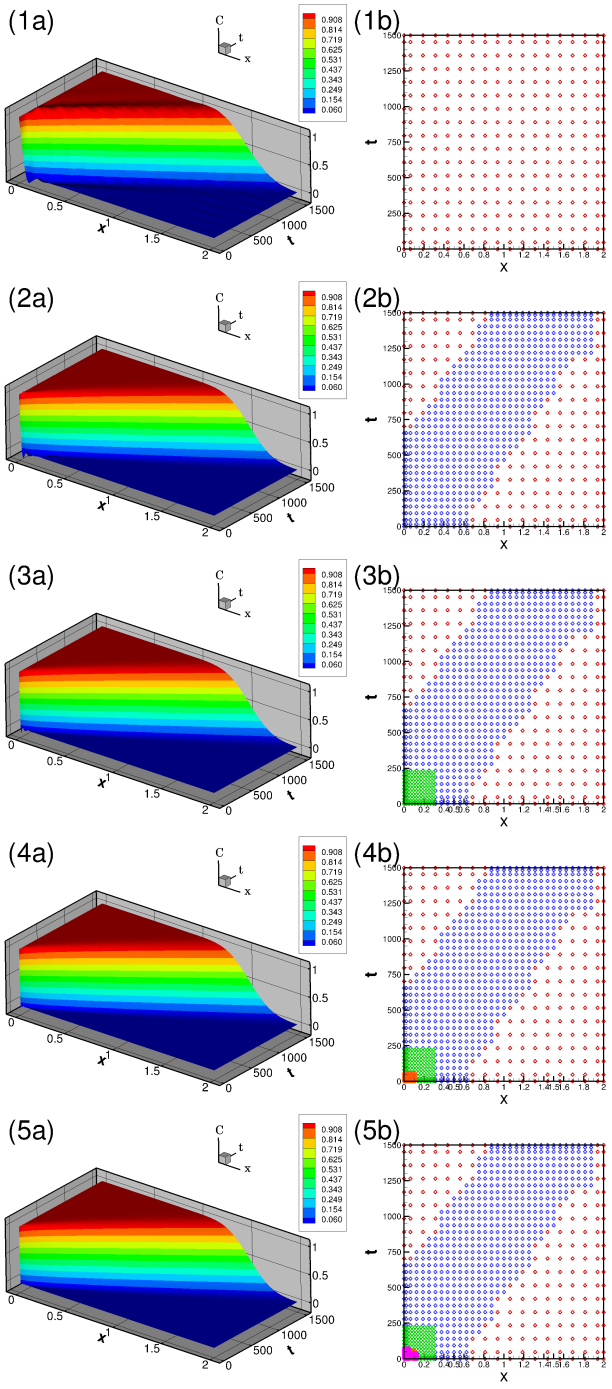

Figure 24: Numerical solution of the ADE (67) at different resolution levels; (1a-5a) HF approximation (without stabilization), (1b-5b) corresponding adaptive time-spatial grids.

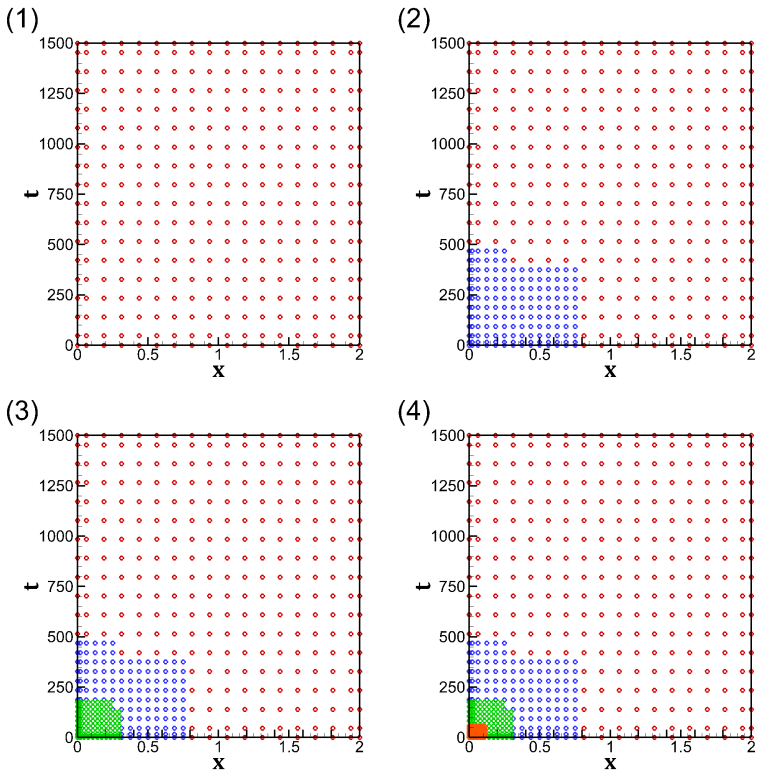

Figure 25: Corresponding adaptive time-spatial grids at different resolution levels of the ADE (67) (with stabilization).

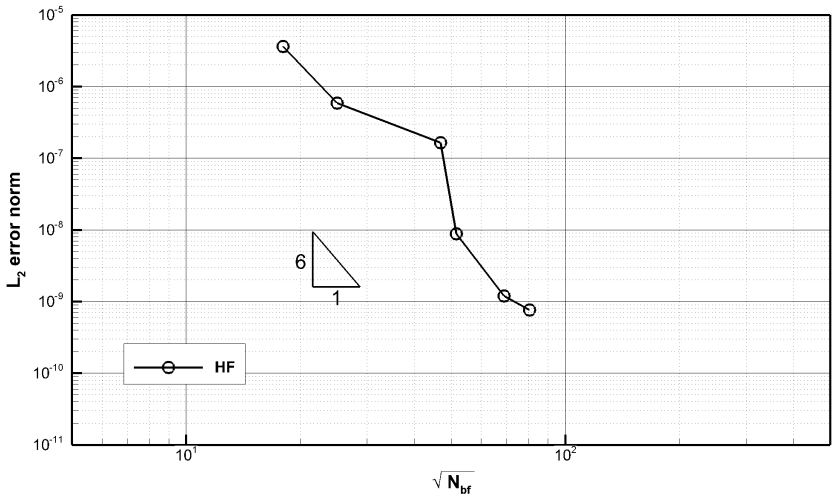

Figure 26: Convergence analysis for adaptive method (without stabilization)

require additional modifications to preserve the essential property of partition of unity that allow easy implementation of local hp-enhancements. Control volume formulation is simple, all control volumes are regular in the parametric space (also related to the Greville collocation points), only overlapping is needed in the zones of contact between different resolution levels.

The developed adaptive algorithm is presented first on a simple example of function approximation for the sake of simplicity of the presented adaptive algorithm, then to the application of the Poisson equation, which has wide implementation in structural and fluid mechanics. On the example of ADE, we show that even in cases when the advective member dominates and creates oscillations in solving using adaptive techniques, we achieve stability and accurate solutions. Even in non-smooth problems, spectral convergence is achieved contrary to the application of uniform grid. CV-IGA ensures local and global mass conservation which is potentially very important for fluid mechanics problems.

Acknowledgments: This research was funded by the Croatian Science Foundation (in Croatian: Hrvatska zaklada za znanost - HRZZ) through the scientific project "Multiphysics modelling of surface-subsurface water systems", grant number: IP-2020-02-2298.

This research is partially supported through project KK.01.1.1.02.0027, a project co-financed by the Croatian Government and the European Union through the European Regional Development Fund - the Competitiveness and Cohesion Operational Programme.

References

[1] A. Brandt, "Multi-Level Adaptive Solutions to Boundary-Value Problems," *Mathematics of Computation*, vol. 31, no. 138, p. 333, 1977.

[2] I. Babushka and W. C. Rheinboldt, "Error Estimates for Adaptive Finite Element Computation," *SIAM J. Num. Anal.*, vol. 15, no. 4, pp. 736–754, 1978.

[3] L. Demkowicz, P. Devloo, and J. Oden, "On an h-type mesh-refinement strategy based on minimization of interpolation errors," *Computer Methods in Applied Mechanics and Engineering*, vol. 53, pp. 67–89, Oct. 1985.

[4] M. J. Berger and P. Colella, "Local adaptive mesh refinement for shock hydrodynamics," *Journal of Computational Physics*, vol. 82, no. 1, pp. 64–84, 1989.

[5] L. Demkowicz, J. Oden, W. Rachowicz, and O. Hardy, "Toward a universal h-p adaptive finite element strategy, part 1. Constrained approximation and data structure," *Computer Methods in Applied Mechanics and Engineering*, vol. 77, pp. 79–112, Dec. 1989.

[6] J. Oden, L. Demkowicz, W. Rachowicz, and T. Westermann, "Toward a universal h-p adaptive finite element strategy, part 2. A posteriori error estimation," *Computer Methods in Applied Mechanics and Engineering*, vol. 77, pp. 113–180, Dec. 1989.

[7] W. Rachowicz, J. Oden, and L. Demkowicz, "Toward a universal h-p adaptive finite element strategy part 3. design of h-p meshes," *Computer Methods in Applied Mechanics and Engineering*, vol. 77, pp. 181–212, Dec. 1989.

[8] A. Harten, "Adaptive Multiresolution Schemes for Shock Computations," 1994.

[9] A. Harten, "Multiresolution algorithms for the numerical solution of hyperbolic conservation laws," *Communications on Pure and Applied Mathematics*, vol. 48, no. 12, pp. 1305–1342, 1995.

[10] C. J. Leo and J. R. Booker, "A boundary element method for analysis of contaminant transport in porous media i: homogeneous porous media," *International Journal for Numerical and Analytical Methods in Geomechanics*, vol. 23, no. 14, pp. 1681–1699, 1999.

[11] F. A. Tavarez and M. E. Plesha, "Discrete element method for modelling solid and particulate materials," *International Journal for Numerical Methods in Engineering*, vol. 70, no. 4, pp. 379–404, 2007.

[12] T. Hughes, J. Cottrell, and Y. Bazilevs, "Isogeometric analysis: Cad, finite elements, nurbs, exact geometry and mesh refinement," *Computer Methods in Applied Mechanics and Engineering*, vol. 194, no. 39, pp. 4135 – 4195, 2005.

[13] T. W. Sederberg, D. L. Cardon, G. T. Finnigan, N. S. North, J. Zheng, and T. Lyche, "T-spline simplification and local refinement," *ACM Trans. Graph.*, vol. 23, pp. 276–283, Aug. 2004.

[14] C. Giannelli, B. Jüttler, and H. Speleers, "Thb-splines: The truncated basis for hierarchical splines," *Computer Aided Geometric Design*, vol. 29, no. 7, pp. 485 – 498, 2012. Geometric Modeling and Processing 2012.

[15] J. A. Cottrell, T. J. R. Hughes, and Y. Bazilevs, "Isogeometric Analysis Toward Intergration of CAD and FEA," p. 335, 2009.

[16] H. Gotovac, L. Malenica, and B. Gotovac, "Control volume isogeometric analysis for groundwater flow modeling in heterogeneous porous media," *Advances in Water Resources*, vol. 148, p. 103838, 2021.

[17] M.-C. Hsu, C. Wang, F. Xu, A. J. Herrema, and A. Krishnamurthy, "Direct immersogeometric fluid flow analysis using b-rep cad models," *Computer Aided Geometric Design*, vol. 43, pp. 143–158, 2016. Geometric Modeling and Processing 2016.

[18] V. L. Rvachev and T. I. Sheiko, "R-Functions in Boundary Value Problems in Mechanics," *Applied Mechanics Reviews*, vol. 48, pp. 151–188, 04 1995.

[19] K. Höllig, C. Apprich, and A. Streit, "Introduction to the web-method and its applications," *Advances in Computational Mathematics*, vol. 23, pp. 215 – 237, 2005.

[20] J. A. Cottrell, T. J. R. Hughes, and A. Reali, "Studies of refinement and continuity in isogeometric structural analysis," *Computer Methods in Applied Mechanics and Engineering*, vol. 196, pp. 4160–4183, Sept. 2007.

[21] Y. W. Bekele, T. Kvamsdal, A. M. Kvarving, and S. Nordal, "Adaptive isogeometric finite element analysis of steady-state groundwater flow," *International Journal for Numerical and Analytical Methods in Geomechanics*, vol. 40, pp. 738–765, Apr. 2016.

[22] G. Lorenzo, M. Scott, K. Tew, T. Hughes, and H. Gomez, "Hierarchically refined and coarsened splines for moving interface problems, with particular application to phase-field models of prostate tumor growth," *Computer Methods in Applied Mechanics and Engineering*, vol. 319, pp. 515–548, June 2017.

[23] A.-V. Vuong, C. Giannelli, B. Jüttler, and B. Simeon, "A hierarchical approach to adaptive local refinement in isogeometric analysis," *Computer Methods in Applied Mechanics and Engineering*, vol. 200,

pp. 3554–3567, Dec. 2011.

[24] D. C. Thomas, M. A. Scott, J. A. Evans, K. Tew, and E. J. Evans, "Bézier projection: A unified approach for local projection and quadrature-free refinement and coarsening of NURBS and T-splines with particular application to isogeometric design and analysis," *Computer Methods in Applied Mechanics and Engineering*, vol. 284, pp. 55–105, Feb. 2015.

[25] Y. Zhang, W. Wang, and T. J. Hughes, "Solid t-spline construction from boundary representations for genus-zero geometry," *Computer Methods in Applied Mechanics and Engineering*, vol. 249-252, pp. 185 – 197, 2012. Higher Order Finite Element and Isogeometric Methods.

[26] Y. Zhang, W. Wang, and T. J. R. Hughes, "Conformal solid t-spline construction from boundary t-spline representations," *Computational Mechanics*, vol. 51, pp. 1051 – 1059, 2013.

[27] X. Wei, Y. Zhang, L. Liu, and T. J. Hughes, "Truncated t-splines: Fundamentals and methods," *Computer Methods in Applied Mechanics and Engineering*, vol. 316, pp. 349 – 372, 2017. Special Issue on Isogeometric Analysis: Progress and Challenges.

[28] H. Casquero, L. Liu, Y. Zhang, A. Reali, and H. Gomez, "Isogeometric collocation using analysis-suitable t-splines of arbitrary degree," *Computer Methods in Applied Mechanics and Engineering*, vol. 301, pp. 164 – 186, 2016.

[29] H. Casquero, L. Liu, Y. Zhang, A. Reali, J. Kiendl, and H. Gomez, "Arbitrary-degree t-splines for isogeometric analysis of fully nonlinear kirchhoff–love shells," *Computer-Aided Design*, vol. 82, pp. 140 – 153, 2017. Isogeometric Design and Analysis.

[30] X. Wei, Y. Zhang, T. J. Hughes, and M. A. Scott, "Truncated hierarchical catmull–clark subdivision with local refinement," *Computer Methods in Applied Mechanics and Engineering*, vol. 291, pp. 1 – 20, 2015.

[31] X. Wei, Y. J. Zhang, T. J. Hughes, and M. A. Scott, "Extended truncated hierarchical catmull–clark subdivision," *Computer Methods in Applied Mechanics and Engineering*, vol. 299, pp. 316 – 336, 2016.

[32] M. Carraturo, C. Giannelli, A. Reali, and R. Vázquez, "Suitably graded thb-spline refinement and coarsening: Towards an adaptive isogeometric analysis of additive manufacturing processes," *Computer Methods in Applied Mechanics and Engineering*, vol. 348, pp. 660 – 679, 2019.

[33] D. D'Angella, S. Kollmannsberger, E. Rank, and A. Reali, "Multi-level bézier extraction for hierarchical local refinement of isogeometric analysis," *Computer Methods in Applied Mechanics and Engineering*, vol. 328, pp. 147 – 174, 2018.

[34] X. Li, X. Wei, and Y. J. Zhang, "Hybrid non-uniform recursive subdivision with improved convergence rates," *Computer Methods in Applied Mechanics and Engineering*, vol. 352, pp. 606 – 624, 2019.

[35] K. A. Johannessen, F. Remonato, and T. Kvamsdal, "On the similarities and differences between classical hierarchical, truncated hierarchical and lr b-splines," *Computer Methods in Applied Mechanics and Engineering*, vol. 291, pp. 64 – 101, 2015.

[36] V. L. Rvachev and V. A. Rvachev, "On a finite function," *Dokl. Akad. Nauk Ukrainian SSR, ser. A*, no. 6, pp. 705–707., 1971.

[37] B. Gotovac, *Numerical modelling of engineering problems by smooth finite functions (In Croatian)*. PhD thesis, 1986.

[38] G. Beylkin and J. M. Keiser, "On the adaptive numerical solution of nonlinear partial differential equations in wavelet bases," *Journal of Computational Physics*, vol. 132, no. 2, pp. 233 – 259, 1997.

[39] V. Kozulić, *Numerical modelling by the fragment method with Rbf functions (In Croatian)*. PhD thesis, 1999.

[40] B. Gotovac and V. Kozulić, "On a selection of basis functions in numerical analyses of engineering problems," *International Journal for Engineering Modelling*, vol. 12, no. 1-4, pp. 25–41, 1999.

[41] V. F. Kravchenko, M. A. Basarab, V. I. Pustovoit, and H. Pérez-Meana, "New constructions of weight windows based on atomic functions in problems of speech-signal processing," *Doklady Physics*, vol. 46, pp. 166 – 172, 2001.

[42] B. Gotovac and V. Kozulić, "Numerical solving of initial-value problems by rbf basis functions," *Structural Engineering and Mechanics*, vol. 14, no. 3, pp. 263–285, 2002.

[43] V. Kozulić and B. Gotovac, "Numerical analyses of 2d problems using fupn (x, y) basis functions," *International Journal for Engineering Modelling*, vol. 13, no. 1-2, pp. 7–18, 2000.

[44] H. Gotovac, R. Andricevic, B. Gotovac, V. Kozulić, and M. Vranjes, "An improved collocation method for solving the henry problem," *Journal of Contaminant Hydrology*, vol. 64, no. 1, pp. 129 – 149, 2003.

[45] H. Gotovac, V. Cvetkovic, and R. Andricevic, "Adaptive fup multi-resolution approach to flow and advective transport in highly heterogeneous porous media: Methodology, accuracy and convergence," *Advances in Water Resources*, vol. 32, no. 6, pp. 885 – 905, 2009.

[46] L. Malenica, H. Gotovac, G. Kamber, S. Simunovic, S. Allu, and V. Divic, "Groundwater flow modeling in karst aquifers: Coupling 3d matrix and 1d conduit flow via control volume isogeometric analysis experimental verification with a 3d physical model," *Water*, vol. 10, no. 12, 2018.

[47] G. Kamber, H. Gotovac, V. Kozulić, L. Malenica, and B. Gotovac, "Adaptive numerical modeling using the hierarchical fup basis functions and control volume isogeometric analysis," *International Journal for Numerical Methods in Fluids*, vol. 92, no. 10, pp. 1437–1461, 2020.

[48] C. Giannelli, B. Jüttler, and H. Speleers, "Strongly stable bases for adaptively refined multilevel spline spaces," *Adv. Comput. Math.*, vol. 40, p. 459–490, Apr. 2014.

[49] R. Kraft, *Adaptive and linearly independent multilevel B-splines*. SFB 404, Geschäftsstelle, 1997.

[50] L. Malenica, *Numerical Modeling Based on Spline Basis Functions: Application to Groundwater Flow Modeling in Karst Aquifers and Advection Dominated Problems*. PhD thesis, 2019.

[51] D. Schillinger, J. A. Evans, A. Reali, M. A. Scott, and T. J. Hughes, "Isogeometric collocation: Cost comparison with Galerkin methods and extension to adaptive hierarchical NURBS discretizations," *Computer Methods in Applied Mechanics and Engineering*, vol. 267, no. February, pp. 170–232, 2013.

[52] S. V. Patankar, *Numerical heat transfer and fluid flow*. Hemisphere Pub. Corp., 1980.

[53] R. W. Johnson, "Higher order b-spline collocation at the greville abscissae," *Applied Numerical Mathematics*, vol. 52, no. 1, pp. 63 – 75, 2005.

[54] H. Gotovac, R. Andricevic, and B. Gotovac, "Multi-resolution adaptive modeling of groundwater flow and transport problems," *Advances in Water Resources*, vol. 30, no. 5, pp. 1105–1126, 2007.

[55] D. Hendriana, "On finite element and control volume upwinding methods for high peclet number flows," Master's thesis, Massachusetts Institute of Technology. Dept. of Mechanical Engineering, 1994.

[56] J. Oden and A. Patra, "A parallel adaptive strategy for hp finite element computations," *Computer Methods in Applied Mechanics and Engineering*, vol. 121, no. 1, pp. 449 – 470, 1995.

[57] W. F. Mitchell, "A collection of 2d elliptic problems for testing adaptive grid refinement algorithms," *Applied Mathematics and Computation*, vol. 220, pp. 350 – 364, 2013.

[58] C. Swaminathan and V. Voller, "Streamline upwind scheme for control-volume finite elements, part i. formulations," *Numerical Heat Transfer, Part B: Fundamentals*, vol. 22, no. 1, pp. 95–107, 1992.

[59] C. Swaminathan, V. Voller, and S. Patankar, "A streamline upwind control volume finite element method for modeling fluid flow and heat transfer problems," *Finite Elements in Analysis and Design*, vol. 13, no. 2, pp. 169–184, 1993.